CHINA CDC WEEKLY

CCDCweekly

Vol. 6 No. 2 Jan. 12, 2024

中 国 疾 病 预 防 控 制 中 心 周 报

A significant decrease in dental
fluorosis among children in endemic
areas of China between 2009 to 2022

2009
34. 87%

2022
10. 19%

Water safety
policy

Health education

Containment measures
implementation

Continuous surveillance on fluorosis

Preplanned Studies

CHINESE CENTER FOR DISEASE CONTROL AND PREVENTION

Cover Image: credited from this week's author Junrui Pei.

Preplanned Studies

Spatial-Temporal Analysis of Drinking Water Type of Endemic Fluorosis — China, 2009–2022

Lijun Zhao[1,2]; Zhe Li[1,2]; Mang Li[1,2]; Hongna Sun[1,2]; Wei Wei[1,2]; Lin Gao[1,2]; Qiaoshi Zhao[1,2]; Yang Liu[1,2]; Xiaohong Ji[1,2]; Cheng Li[1,2]; Jian Wang[1,2]; Yanhui Gao[1,2]; Junrui Pei[1,2,#]

Summary

What is already known about this topic?

Endemic fluorosis, caused by high fluoride levels in drinking water, has been a significant health issue in rural areas of China for many decades.

What is added by this report?

There has been a notable decline in the detection rate of dental fluorosis in children aged 8–12 years in drinking water fluorosis areas across the country from 2009 to 2022. While 14 provincial-level administrative divisions are classified as low-probability clusters, Tianjin remains classified as a high-probability cluster.

What are the implications for public health practice?

The current policy for preventing and controlling endemic fluorosis in China needs adjustment. Rather than focusing solely on regions with high incidence, there should be a shift towards monitoring and early warning of fluoride exposure. Additionally, local containment measures should be intensified.

Drinking water type of endemic fluorosis, also known as drinking water fluorosis, is a chronic condition that occurs when individuals consume high-fluoride water over an extended period. This leads to the development of dental and skeletal fluorosis (*1*). Drinking water fluorosis is a global issue, affecting over 60 countries and regions. It poses a significant public health concern in 25 countries, impacting approximately 200 million individuals (*2*). In China, drinking water fluorosis is a prevalent form of endemic fluorosis, affecting 28 provincial-level administrative divisions (PLADs) and more than 70,000 villages (*3*). It is an urgent public health problem, particularly in rural areas. Over the past twenty years, rural safe water projects have been implemented by central and local governments to prevent and control drinking water fluorosis. However, there is limited information regarding the national-level temporal and spatial distribution of this disease in recent years. Therefore,

our study aimed to investigate the prevalence of dental fluorosis in drinking water fluorosis areas in China from 2009 to 2022. We found a significant decrease in the detection rate of dental fluorosis in children aged 8–12 years nationwide. Additionally, 14 PLADs were classified as low probability clusters, while Tianjin remained a high probability cluster. These findings provide valuable insights for national adjustments to drinking water fluorosis prevention and control strategies.

The study data were obtained from the Surveillance Report of the Endemic Disease Control Center of the China CDC. The data collected spanned from 2009 to 2022 and focused on the detection rate of dental fluorosis in children aged 8–12 years in 27 PLADs of China, with the exception of Xizang.

We used an Autoregressive Integrated Moving Average (ARIMA) model to analyze national children's dental fluorosis detection rates from 2009–2018. The ARIMA model was constructed using the Augmented Dickey-Fuller test with the Stats package in R [version 4.3.1; R Core Team (2020). R: A language and environment for statistical computing. R Foundation for Statistical Computing, Vienna, Austria] to assess the effectiveness of prevention and control measures. We analyzed the smoothness of the logit-transformed detection rate and the residuals of the model were tested with the Ljung-Box model (*P*>0.05) to determine white noise. The Bayesian information criterion (BIC) was used to select the best model fit.

Additionally, we performed spatial analysis on the detection rates of dental fluorosis in children from 2009 to 2022 to examine geographic aggregation. The Local indicators of spatial autocorrelation (LISA) analysis was conducted using GeoDa (version 1.20.0; GeoDa Institute) software to calculate global and local Moran's indices (Moran's I value).

Finally, the space-time interaction of dental fluorosis detection rates among children in each province from 2009 to 2022 was analyzed using SaTScan (version 10.1; GeoDa Institute). A moving scanning window

method was employed, with a circular window at the bottom varying in radius from 0 to 50% of the total population, and the log-likelihood ratio (LLR) was used as the statistic. A higher LLR indicated a higher likelihood of an area being an agglomeration area. The odds ratio (*OR*) for the area was then calculated and tested for statistical significance using the Global Space-Time Interaction Tests, with a test level of α =0.05.

From 2009 to 2022, the prevalence of dental fluorosis among children aged 8–12 years in areas of China with endemic fluorosis of drinking water showed a consistent decrease. The detection rate decreased from 34.87% in 2009 to 10.19% in 2022 (Table 1). In China, the control standard for endemic fluorosis areas sets a target detection rate of less than 30% in children aged 8–12 years. Additionally, a limit of 15% is used for the assessment of eliminating coal-burning type of endemic fluorosis. In 2013, the detection rate fell below 30% for the first time, and in 2020 it fell below 15%. The monitoring data for the detection rate of children's dental fluorosis aligned closely with the predicted values from 2009 to 2018 using the ARIMA model. However, the difference between the monitoring and predicted values widened significantly in 2019–2022, ranging from 5.42% in 2019 to 7.56% in 2022 (Table 1).

The analysis of global aggregation indicated that except for 2012, the global Moran's I values for the overall detection rates of dental fluorosis in children from 2009 to 2022 were positive. Among these, only in 2009, the statistic was found to be significant (Z=1.8811, *P*=0.040), suggesting that the degree of global aggregation followed a random pattern, except for 2009, which showed an aggregated pattern (Table 2).

The local aggregation analysis revealed consistent types of aggregation and geographical distribution across different years. In 2014, a High-high aggregation area was identified in Shanxi, and the northern region consistently showed Low-high aggregation areas in Beijing for six years and in Shandong in 2019. High-low aggregation areas were predominantly located in the southern region, with cases observed in Guangxi for four years and Jiangxi in 2010. The majority of years saw Low-low aggregation areas covering several southern PLADs, including eleven years in Hunan, eight years in Guangdong, seven years in Jiangxi, and two years in both Fujian and Guangxi (Table 2).

After global space-time interaction tests of the

TABLE 1. Monitoring values and ARIMA model predictions of dental fluorosis detection rate in children aged 8–12 years in drinking water fluorosis areas — China, 2009–2022.

Year	Detection rates of dental fluorosis in children (%)		
	Monitoring value	Fitted/predicted value	95% *CI*
2009	34.87	34.88	–
2010	33.98	34.45	–
2011	32.78	33.22	–
2012	30.81	31.75	–
2013	28.58	29.54	–
2014	27.74	27.29	–
2015	26.55	26.52	–
2016	25.98	25.40	–
2017	22.95	24.80	–
2018	22.07	21.75	–
2019	15.50	20.92	(19.49–22.43)
2020	13.60	19.82	(17.82–22.00)
2021	10.84	18.77	(16.34–21.46)
2022	10.19	17.75	(14.99–20.90)
MAPE	–	2.67	–
R²	–	0.97	–

Abbreviation: ARIMA=autoregressive integrated moving average; MAPE=mean absolute percentage error; *CI*=confidence interval.
"–" indicates no statistic analysis for this year or this index.

detection rate of dental fluorosis among children aged 8–12 years from 2009 to 2022, three clusters were found, including one high-prevalence and two low-prevalence clusters, as shown in Table 3. Among them, the high-prevalence cluster was in Tianjin (LLR=88,828.30, *P*<0.001). The total number of dental fluorosis cases detected in Tianjin from 2017–2022 was more than that of the expected cases, and the *OR* was 2.98. Conversely and apparently, two low-prevalence clusters covered more PLADs, except that in the northeast, and the clustering time was between 2019 and 2022. One low-prevalence cluster was distributed in Henan, Shanxi, and Shandong in 2021–2022 (LLR=21,423.60, *P*<0.001), with the total number of cases of dental fluorosis detected less than the expected one, and the *OR* is 0.58. The other low-prevalence cluster was relatively widely distributed in 11 PLADs, and the *OR* is 0.34 (LLR=40,118.60, *P*<0.001) (Table 3).

DISCUSSION

This study demonstrates the effective control of dental fluorosis in children residing in areas of China

TABLE 2. Global aggregation analysis and local aggregation areas of dental fluorosis detection rate in children aged 8–12 years in drinking water fluorosis PLADs — China, 2009–2022.

Year	Global aggregation analysis			Localized areas of aggregation			
	Moran's I	Z	P value	High-high agglomeration	High-low agglomeration	Low-high agglomeration	Low-low agglomeration
2009	0.190	1.8811	0.040				Hunan, Jiangxi, Guangdong
2010	0.068	−0.1753	0.465		Jiangxi		
2011	0.008	0.3415	0.344		Guangxi		Hunan, Jiangxi
2012	−0.083	−0.3609	0.377		Guangxi		
2013	0.048	0.6778	0.243			Beijing	Hunan, Jiangxi, Guangdong, Guangxi
2014	0.121	1.2050	0.126	Shanxi			Hunan, Jiangxi, Guangdong, Guangxi
2015	0.052	0.7362	0.234		Guangxi		Hunan, Jiangxi
2016	0.035	0.5698	0.274		Guangxi		Hunan
2017	0.065	0.8128	0.206			Beijing	Hunan, Jiangxi, Guangdong, Guangxi
2018	0.120	1.2333	0.117				Hunan, Jiangxi, Guangdong
2019	0.132	1.5438	0.069			Beijing, Shandong	Hunan, Guangdong
2020	0.084	1.1236	0.147			Beijing	Hunan, Guangdong, Fujian
2021	0.018	0.5549	0.257			Beijing	Hunan, Jiangxi, Guangdong
2022	0.078	1.0321	0.143			Beijing	Hunan, Guangdong, Fujian

Abbreviation: PLADs=provincial-level administrative divisions.

TABLE 3. Global space-time interaction tests for the detection rate of dental fluorosis in children aged 8–12 years in the fluorosis PLADs caused by drinking water fluorosis in China from 2009–2022.

Type of cluster (number)	PLADs	Time (year)	The total number of children detected	The number of fluorosis cases detected	Expected cases	OR	LLR	P value
High-prevalence cluster								
1	Tianjin	2017–2022	554,169	187,221	70,766	2.98	88,828.30	<0.001
Low-prevalence clusters								
11	Yunnan, Guangxi, Chongqing, Sichuan, Hunan, Guangdong, Shaanxi, Gansu, Qinghai, Hubei, Jiangxi	2019–2022	975,218	45,708	124,524	0.34	40,118.60	<0.001
3	Henan, Shanxi, Shandong	2021–2022	1,534,525	122,176	195,940	0.58	21,423.60	<0.001

Abbreviation: OR=odds ratio; LLR=log likelihood ratio; PLADs=provincial-level administrative divisions.

with high levels of fluoride in drinking water. However, variations in the distribution of dental fluorosis exist across different regions and over time. From 2009 to 2022, a significant decrease in the prevalence of dental fluorosis was noted among children aged 8–12 years residing in these areas. In 2014, Shanxi remained in a High-high cluster, while other regions exhibited Low-low, Low-high, or High-low clusters. Although 14 PLADs were identified as

low-probability clusters, Tianjin continued to be classified as a high-probability cluster. The findings of this study have implications for targeted policies, resource allocation, and optimization of prevention and control efforts in relation to the temporal and spatial epidemiological characteristics of drinking water fluorosis.

The analysis of temporal trends indicates a decline in dental fluorosis among children residing in areas with

drinking water fluorosis in China. The observed dental fluorosis detection rates in the period 2019–2022 were significantly lower than the predicted values. The difference between the observed and predicted values increased from 5.42% in 2019 to 7.56% in 2022 with the rate of decrease in an increasing mode, which indicates that the prevention and control of fluorosis in the past five years had significant benefits. This positive outcome can be attributed to the Chinese government's commitment to public health and the implementation of measures outlined in the "Three-year Action Program for the Prevention and Control of Endemic Diseases (2018–2020)". These measures include a focused effort to improve water quality and reduce fluoride content in areas affected by endemic diseases. Consequently, there has been a notable improvement in water quality compliance and a successful control of the risks associated with drinking water fluorosis (4–5).

Spatial analysis revealed that only 2009 exhibited a global aggregation pattern, while all other years displayed a random pattern. Further analysis using LISA identified localized aggregations in different years, primarily concentrated in the southern region of China with low detection rates. This suggests that, apart from the southern region, other regions exhibit a more random distribution, with high detection rates interspersed with low detection rates. The diverse patterns of aggregation across regions may be influenced by the complex geographic environment of China and the varying prevention and control capabilities of each region (6–7).

The results of global space-time interaction tests indicated that the aggregation of dental fluorosis cases was primarily observed in the last five years. Among all the PLADs investigated, only Tianjin exhibited a High-prevalence cluster, while 14 areas showed Low-prevalence clusters. Furthermore, the actual number of children with dental fluorosis in these 14 areas was lower than expected, validating the effectiveness of the three-year endemic disease prevention and control measures (8). Previous studies have highlighted Tianjin as the region most affected by drinking water fluorosis between 2016 and 2020 (9–10). However, our study revealed that the actual number of dental fluorosis cases detected in Tianjin exceeded the expected number, suggesting that the situation in this area remains severe and requires special attention.

This study has several limitations. First, the use of dental fluorosis detection rates in children as a reflection of the prevalence of fluorosis in a region may underestimate the true extent of the condition due to the wide range of symptoms associated with fluorosis in humans. Second, the clinical examination of dental fluorosis is conducted independently by each province, resulting in inevitable differences and a lack of consistency, despite clear judgment criteria. Lastly, this study primarily focuses on PLADs, which prevents the distinction of key areas within each PLAD. Future research should consider further analysis at the county and even township level to better understand the distribution of fluorosis.

Overall, the prevalence of endemic drinking water fluorosis in China has transitioned from a high regional concentration to a lower overall prevalence. As a result, it is necessary to adjust China's prevention and control policies accordingly. Rather than focusing solely on high-incidence regions, efforts should now be directed towards monitoring and early detection of fluoride exposure, as well as implementing stronger prevention and control measures at the local level. The government should adopt a dynamic approach in optimizing the allocation of resources for fluorosis prevention and control, taking into account changes in the spatial distribution of drinking water fluorosis. Additionally, vigilance should be maintained to prevent the re-emergence of fluorosis hazards in regions with random detection rates. It is crucial to identify the causes behind the aggregation of high-prevalence regions and develop tailored plans to effectively implement prevention and control measures, thus mitigating the risks associated with fluorosis.

Conflicts of interest: No conflicts of interest.

Corresponding author: Junrui Pei, peijunrui@ems.hrbmu.edu.cn.

1 Center for Endemic Disease Control, Chinese Center for Disease Control and Prevention; Harbin Medical University, Harbin City, Heilongjiang Province, China; 2 Key Lab of Etiology and Epidemiology, Education Bureau of Heilongjiang Province (23618504), Ministry of Health of PR; Harbin Medical University, Harbin City, Heilongjiang Province, China.

REFERENCES

1. Wei W, Pang SJ, Sun DJ. The pathogenesis of endemic fluorosis: research progress in the last 5 years. J Cell Mol Med 2019;23(4):2333 – 42. http://dx.doi.org/10.1111/jcmm.14185.
2. Li Z, Que WJ, Wang T, Ma YZ, Meng XY, Sowanou A, et al. Current status of global endemic fluorosis and measures for its prevention and control. In: Proceedings of the Eleventh National Conference on Endemic Diseases. China, 2023. Chinese Journal of Endemiology. 2023;42:11. (In Chinese)
3. Center for Endemic Disease Control, Chinese Center for Disease Control and Prevention. The 2020 report of national drinking water endemic fluorosis monitoring: Center for Endemic Disease Control, Chinese Center for Disease Control and Prevention. 2021. [2023-11-23]. https://www.hrbmu.edu.cn/dbzx/fzjc/dfxfzd.htm. (In Chinese)
4. Gao YH. Interpretation of the tasks of the special three-year program for prevention and control of endemic diseases (2018-2020). Chin J Endemiol 2019;38(1):1 – 3. http://dx.doi.org/10.3760/Cma.J.Issn.2095-4255.2019.01.001. (In Chinese).
5. Liu H, Gao YH, Shen HM, Sun DJ. Achievement during the 13th Five-Year Plan and analysis of the 14th Five-Year Plan on prevention and control of endemic diseases in China. Chin J Endemiol 2022;41(3): 176 – 9. http://dx.doi.org/10.3760/Cma.J.Cn231583-20220302-00056. (In Chinese).
6. Liu H, Gao YH. The progress, important experience and ideas for the next step of three-year special program for control of endemic diseases in China. Chin J Endemiol 2020;39(1):1 – 3. http://dx.doi.org/10.3760/cma.j.issn.2095-4255.2020.01.001. (In Chinese).
7. Chang CY. Introduction to the division and characterization of hydrogeological types of coal mines in China. West-China Exploration Eng 2021;33(11):132 – 3. http://dx.doi.org/10.3969/j.issn.1004-5716.2021.11.044. (In Chinese).
8. Gao YH. Endemic disease control effective in helping people in disease areas running for prosperity. China Med News 2021;36(1):12. http://dx.doi.org/10.3760/cma.j.issn.1000-8039.2021.01.111. (In Chinese).
9. Zhang L, Zhao L, Zeng Q, Fu G, Feng BJ, Lin XH, et al. Spatial distribution of fluoride in drinking water and health risk assessment of children in typical fluorosis areas in North China. Chemosphere 2020;239:124811. http://dx.doi.org/10.1016/j.chemosphere.2019.124811.
10. Fan SL. Current prevention and control of endemic fluorosis during the Thirteenth Five-Year Plan in China. J Environ Occup Med 2020;37(12):1219 – 23. http://dx.doi.org/10.13213/j.cnki.jeom.2020.20274. (In Chinese).

Preplanned Studies

The Combined Effects of High Temperatures and Ozone Pollution on Medical Emergency Calls — Jinan City, Shandong Province, China, 2013–2019

Huiyun Chang[1]; Chong Liu[2]; Xingyi Geng[1]; Xiumiao Peng[3]; Ke Huang[4]; Liheng Wang[3]; Liangliang Cui[1,#]

Summary

What is already known about this topic?

Studies have extensively documented the separate and independent effects of extreme temperature and ozone on morbidity and mortality associated with respiratory and circulatory diseases.

What is added by this report?

The study revealed a significant association between elevated temperature, ozone pollution, and the combined effect of high temperature and ozone pollution with an increased risk of all-cause medical emergency calls (MECs) and MECs specifically related to neurological diseases.

What are the implications for public health practice?

Interventional measures should be implemented to mitigate exposure to high temperatures and ozone levels. Specifically, during the warm season, it is crucial for relevant authorities to focus on disseminating scientific information regarding the health impacts of elevated temperatures and ozone pollution. Additionally, timely public health advisories should be issued to alert the public effectively.

Epidemiological evidence demonstrates the significant impact of high temperature on both short-term and long-term health outcomes, resulting in increased morbidity and mortality rates for respiratory and circulatory diseases, among other health conditions (*1*). Simultaneously, there is a growing concern about ozone (O_3) pollution, which poses a pressing challenge to urban development (*2*). Numerous studies have established a strong association between O_3 pollution and the onset and progression of respiratory and circulatory diseases (*3–4*). However, there is still a research gap concerning the combined effects of these two variables. Recently, there has been a growing interest in using medical emergency calls (MECs) as indicators to explore the acute effects of high temperature and O_3 pollution (*5–7*). Addressing this research gap, our study focuses on Jinan City, Shandong Province, China, as a representative urban area grappling with the dual challenge of high temperature and O_3 pollution. We employed a time-stratified case-crossover study design to estimate the impacts of high temperature and O_3 pollution on MECs. The results indicate that high temperature, O_3 pollution, and their combination significantly increase the risk of all-cause MECs and MECs specifically related to neurological diseases. These findings provide essential information for the development of future measures to reduce exposure to high temperature and O_3 pollution. Moreover, emphasizing the necessity to consider the combined effects of high temperature and O_3 pollution is crucial for addressing emerging public health concerns.

For this research study, we collected daily data from the MECs of the Jinan Medical Emergency Center (JMEC) website (http://www.jn120.cn/). The data were collected from May 1 to September 30 for the years 2013–2019. There were minor fluctuations in the MECs rate during the study period, as shown in Supplementary Table S1 (available in https://weekly.chinacdc.cn/). The information obtained from the MECs included the patient's call time, primary statement, and preliminary diagnosis. The primary statement information referred to the main signs and symptoms provided during the telephone call, while the preliminary diagnosis information indicated the disease diagnosis given when the patient was admitted to the hospital's emergency department. JMEC oversees 66 first-aid service stations that are affiliated with hospitals, providing coverage across all ten administrative districts of Jinan City, as shown in Supplementary Table S2 (available in https://weekly.chinacdc.cn/). To classify the MECs, we used the International Classification of Diseases, 10th revision (ICD-10). We specifically screened for ICD-10 codes J00–J99, which are associated with

respiratory diseases, I00–I99, which are related to circulatory diseases, and G00–G99, which pertain to neurological diseases.

Meteorological data collected daily throughout the study period were provided by the China Meteorological Science Data Sharing Service Network (http://data.cma.gov.cn/). This data included the daily mean maximum temperature (℃), relative humidity (%), pressure (hPa), and wind speed (m/s). The daily air pollutant data, such as fine particulate matter ($PM_{2.5}$), particulate matter (PM_{10}), nitrogen dioxide (NO_2), sulfur dioxide (SO_2), carbon monoxide (CO), and 8-hour ozone (O_3-8h, abbreviated as O_3), were obtained from the Jinan Ecological Environmental Protection Bureau. For this study, we determined the daily pollutant concentration level in Jinan by averaging the readings from all monitoring stations.

In the initial stage of our analysis, we began with a descriptive examination of the compiled data using various indicators, including mean, standard deviation, minimum, maximum, median, first quartile, and third quartile. Following this, correlation analysis was conducted to explore the relationship between temperature, ozone concentration, and MECs, as well as the associations between air pollutants and meteorological factors. Subsequently, a time-stratified case-crossover study design in combination with a

conditional logistic regression model was employed to investigate the acute impacts of temperature and ozone pollution on MECs. Detailed information and sensitivity analyses for this core model can be found in the Supplementary Material (available in https://weekly.chinacdc.cn/). Based on a comprehensive review of previous studies and our analytical results, we selected a five-day period for our lag effect study. We examined the effects on the current day (Lag0), single-day lag effects (Lag1–Lag5), and cumulative lag effects (Lag01–Lag05) on MECs to identify the most impactful day and estimate the effect. The effect estimates were presented as odds ratios (ORs) along with their corresponding 95% confidence intervals (CIs). To address diseases with high sensitivity, a subgroup analysis focusing specifically on respiratory, circulatory, and neurological diseases was conducted. The R software (version R 4.2.0; R Studio Inc; the USA) was used for the analysis of time-stratified cross-case data. Statistical significance was considered at a P-value of less than 0.05.

Table 1 presents the daily levels of air pollutants, meteorological factors, and MECs in Jinan from 2013 to 2019. The total number of MECs recorded during this period was 275,868, with an average daily number of all-cause MECs at 258±40 cases. Among these cases, the number of MECs related to respiratory,

TABLE 1. Daily levels of air pollutants, meteorological factors, and MECs in Jinan City from 2013 to 2019.

Variables	Mean±SD	Min	P_{25}	P_{50}	P_{75}	Max
Air pollution (μg/m³)						
PM_{10}	57.09±28.72	3	36	51	73	196
$PM_{2.5}$	114.83±51.03	5	79	106	141	348
NO_2	38.13±12.56	9	29	36	45	88
SO_2	30.09±22.88	6	14	24	39	182
CO	969.75±324.51	363	735	910	1,116	2,598
O_3	154.67±47.87	30	122	157	187	266
Meteorological factor						
Temperature (℃)	30.38±4.06	15.6	27.9	30.9	33.3	39.9
Wind speed (m/s)	2.36±1.02	0.4	1.7	2.1	2.8	7.7
Relative humidity (%)	61.34±17.37	15	49	62	74	98
Pressure (hPa)	988.53±5.18	975	985	987	992	1,004
Medical emergency calls (calls/day)						
All-cause	258±40	161	230	252	278	395
Respiratory diseases	19±9	2	11	18	25	44
Cardiovascular diseases	35±10	6	28	35	42	63
Neurological diseases	39±8	15	33	39	44	78

Abbreviation: MECs=medical emergency calls; SD=standard deviation; Min=minimum; P_{25}=25th percentile; P_{50}=50th percentile; P_{75}=75th percentile; Max=maximum.

circulatory, and neurological diseases were 19±9, 35±10, and 39±8, respectively. Furthermore, the average maximum daily temperature reached 30.38±4.06 ℃, while the daily concentration of O_3 was 154.67±47.87 μg/m³.

The chronological diagram presented in Supplementary Figure S1 (available in https://weekly.chinacdc.cn/) visually demonstrates consistent trends and potential relationships among temperature, O_3 concentration, and MECs. Additionally, the Spearman correlation analysis (Figure 1) indicates statistically significant correlations between these variables during the study period. Specifically, temperature and MECs, O_3 concentration and MECs, and temperature and O_3 concentration exhibited significant correlations. Notably, a strong positive correlation was observed between O_3 concentration and temperature (r=0.63, P<0.05). Further details on the correlation results between air pollutants and meteorological factors are provided in Supplementary Table S3 (available in https://weekly.chinacdc.cn/).

Figure 2 presents an analysis of the single-day lag effect concerning temperature, O_3 pollution, and their combined impact. Statistically significant independent effects of both temperature and O_3 pollution on all-cause MECs were noted from Lag0 to Lag3, with the most pronounced effect occurring at Lag0. The *OR* values for temperature and O_3 pollution were 1.013 (95% *CI*: 1.010, 1.015) and 1.0005 (95% *CI*: 1.0002, 1.0006), respectively. Notably, the combined influence of temperature and O_3 pollution demonstrated statistical significance from Lag0 to Lag5, peaking at Lag0, with an *OR* of 1.017 (95% *CI*: 1.010, 1.024). A trend of marginal decline in *OR* values was observed for both independent and combined effects of temperature and O_3 pollution with progressing Lag days. Additionally, subgroup analysis indicated significant impacts on MECs for neurological diseases, with *OR* values of 1.017 (95% *CI*: 1.010, 1.024), 1.001 (95% *CI*: 1.000, 1.002), and 1.022 (95% *CI*: 1.004, 1.041). However, the effects of MECs on respiratory and circulatory diseases were not statistically significant. The cumulative lag effect analysis of temperature, O_3 pollution, and their combined effect is depicted in Supplementary Figure S2 (available in https://weekly.chinacdc.cn/).

DISCUSSION

This study employs a time-stratified case-crossover design to investigate the combined effects of high temperature and O_3 pollution on MECs within Jinan City from 2013 to 2019. The results of our analysis confirm that both temperature and O_3 pollution independently increase the risk of MECs during the warm season, and their combined influence further escalates this risk. These findings differ somewhat from previous research studies (*6–7*). From a pathogenesis perspective, it is understood that both temperature and O_3 pollution can contribute to the development and occurrence of various respiratory, circulatory, and neurological disorders. This may occur through mechanisms such as inflammation and immune dysregulation. However, it is important to consider that regional disparities in weather conditions (such as temperature, humidity, and wind speed), demographic characteristics of the at-risk population, the composition of O_3 pollution sources, and the range of O_3 concentrations could account for the observed discrepancies. Additionally, variations in exposure durations and statistical analysis models may also play significant roles in explaining the differences encountered.

The results of the stratified analysis indicate that both temperature and O_3 pollution have a positive influence on neurological disorders in residents. This can be attributed to the reactive nature of O_3, an oxidant and reactive oxygen species. When inhaled, O_3 reacts with proteins and lipids, leading to the production of denatured proteins/lipids, carbon/oxygen free radicals, and toxic compounds. This triggers an oxidative stress response in lung macrophages, resulting in physiological disruptions (*8*). Additionally, higher temperatures exacerbate this issue by promoting immune cell activation and transition, leading to various immune adaptations that contribute to the development of neurological diseases (*9*). Interestingly, surface-level O_3 formation rates are closely linked to temperature, suggesting potential reciprocal influences between O_3 pollution and climate change. Therefore, the combination of these factors has a significant impact on population health. However, previous studies have primarily focused on the independent effects of meteorological factors or air pollution on neurological diseases. Hence, this study's examination of the combined implications of temperature and O_3 pollution on neurological diseases is of utmost importance. It is recommended that future research further investigates the risks associated with temperature and O_3 pollution on various neurological disorders, while also considering disease-specific sensitivities.
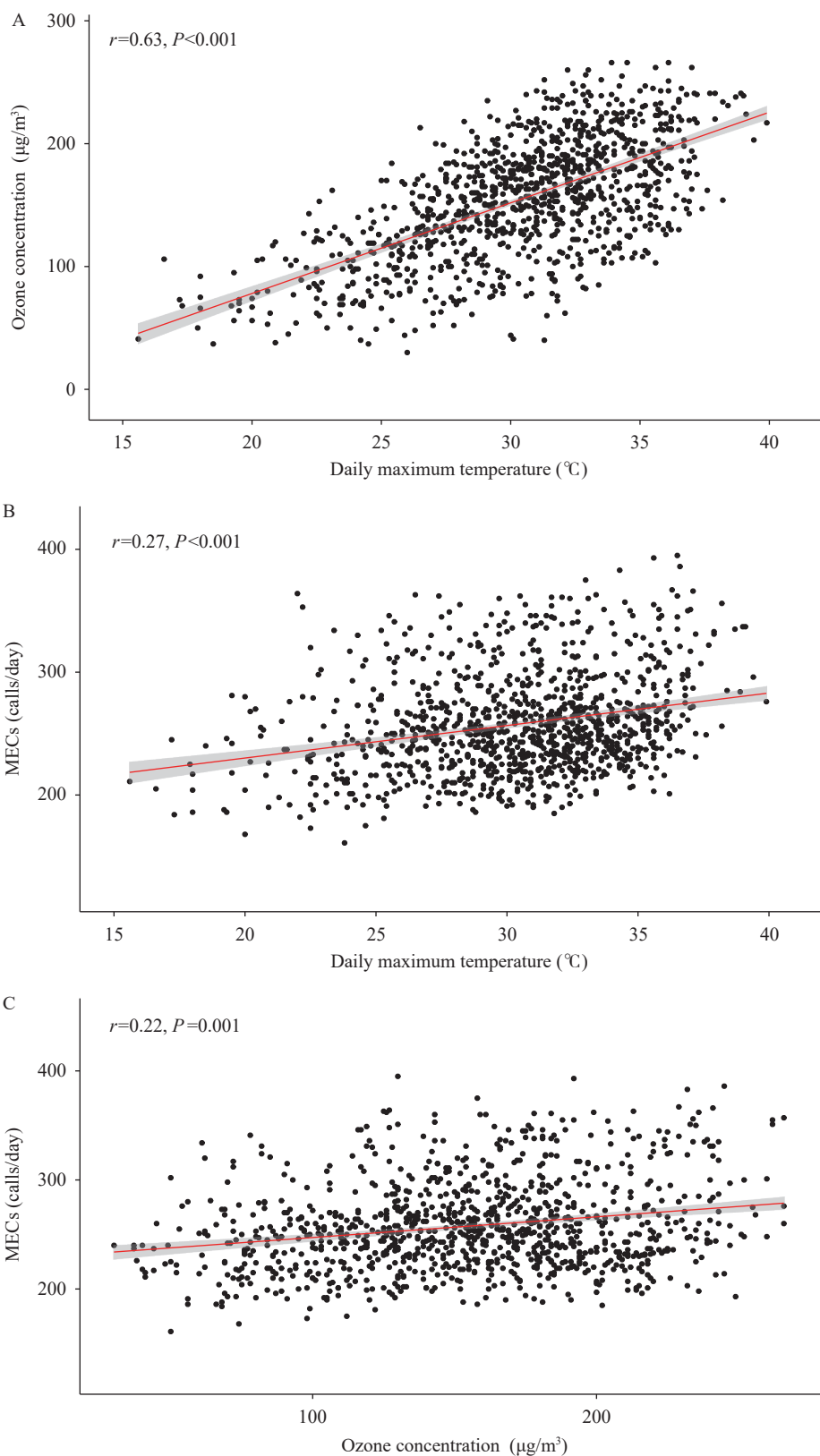
FIGURE 1. Spearman correlation analysis between temperature, O₃, and MECs in Jinan from May to September 2013–2019. (A) represents the correlation analysis between O₃ and temperature; (B) represents the correlation analysis between temperature and MECs; (C) represents the correlation analysis between O₃ and MECs.
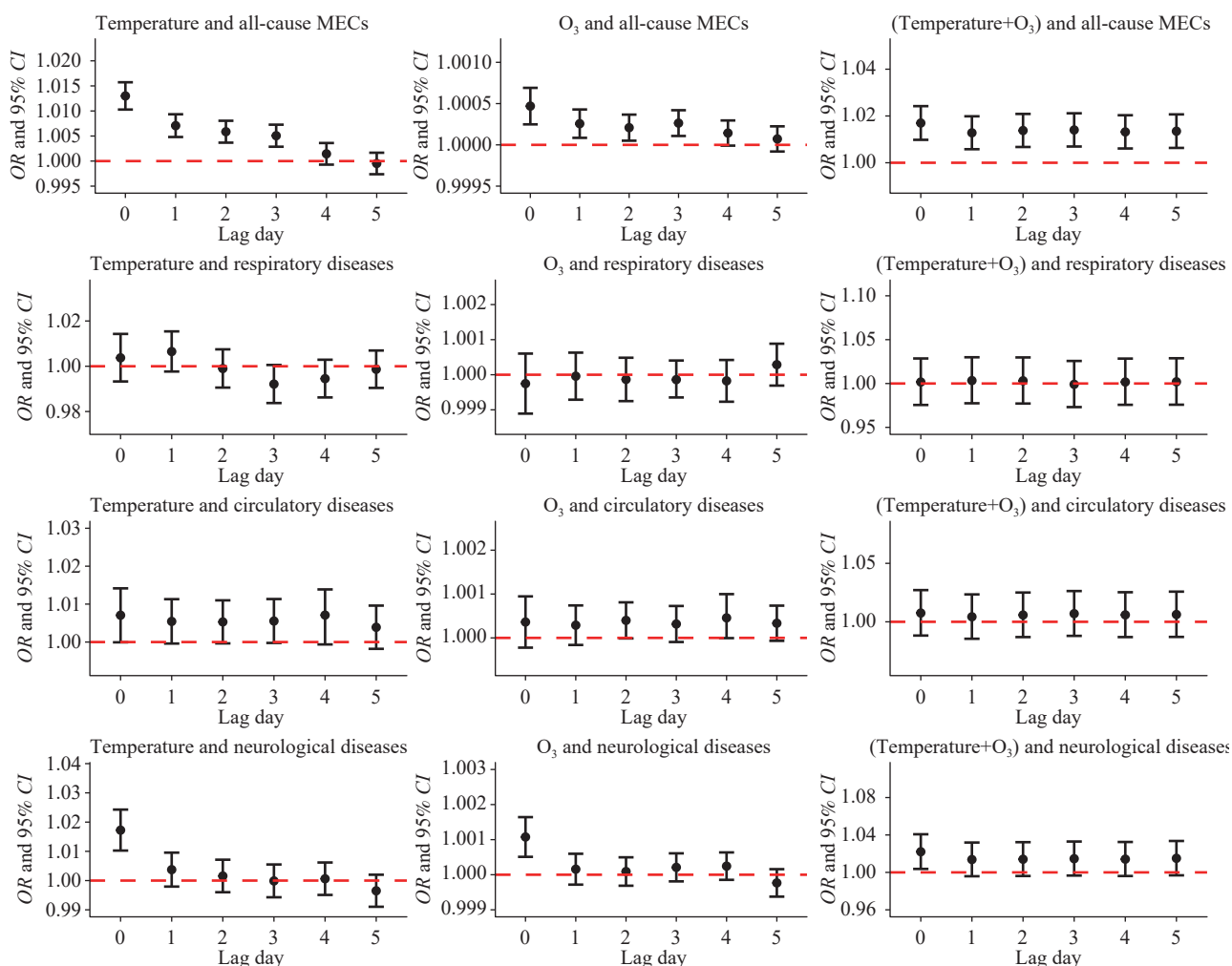
FIGURE 2. The lag effects of temperature, ozone (O₃), and their combined effects on all-cause morbidity and morbidity rates for various systemic diseases during the warm season in Jinan from 2013 to 2019.
Note: The variable "Temperature+O₃" in this study represents the combined impact of high temperature and ozone pollution.
Abbreviation: OR=odds ratio; CI=confidence interval; MECs=medical emergency calls.

In our stratified analysis, we have also found that the combined effect of warm season temperature and ozone pollution on emergency calls for respiratory and circulatory diseases was not statistically significant. This finding contradicts previous research (6–7). The apparent discrepancies in research outcomes might be attributed to variations in research design methodologies, geographic differences in warm season temperature ranges and levels of O_3 pollution, as well as variations in the characteristics of the study populations, all of which may influence the direction of the study's impact.

However, this study has several limitations that should be considered. Firstly, the use of urban monitoring data averages to represent individual exposure levels may introduce variability into the estimates of combined effects on study outcomes.

Secondly, the study was unable to investigate the susceptibility of different genders and age groups, which could have provided valuable insights into the potential heterogeneity of the effects. Thirdly, it should be noted that this study assumes Jinan City is representative of other cities, and outcomes may differ in cities with diverse geographical locations and climate patterns. Lastly, since the COVID-19 epidemic in 2020, the disease composition of MECs has changed significantly, so this study only analyzes data up to 2019.

In conclusion, there was a significant rise in heat-related morbidity cases among residents due to the combined impact of high temperature and O_3 pollution. Of particular concern were the increased incidences of neurological disorders associated with these environmental factors. These findings highlight

the urgent need for increased awareness and action from relevant agencies. During the peak of summer, it is crucial to prioritize the dissemination of scientific knowledge regarding meteorological factors and the health implications of O_3 pollution. Specifically, when faced with elevated temperatures and heightened O_3 levels, it becomes imperative for authorities to issue public health warnings as a proactive measure in order to reduce potential health risks.

Conflicts of interest: All authors had no conflicts of interest.

Corresponding author: Liangliang Cui, cll602@163.com.

¹ Department of Scientific Research and Education, Jinan Municipal Center for Disease Control and Prevention, Jinan Municipal Center for Disease Control and Prevention Affiliated to Shandong University, Jinan City, Shandong Province, China; ² Jinan Health Well Development Center, Jinan City, Shandong Province, China; ³ Department of Environmental Health, Jinan Municipal Center for Disease Control and Prevention, Jinan City, Shandong Province, China; ⁴ Department of Emergency, Jinan Medical Emergency Center, Jinan City, Shandong Province, China.

REFERENCES

1. Cheng J, Xu ZW, Bambrick H, Prescott V, Wang N, Zhang YZ, et al. Cardiorespiratory effects of heatwaves: a systematic review and meta-analysis of global epidemiological evidence. Environ Res 2019;177: 108610. http://dx.doi.org/10.1016/j.envres.2019.108610.
2. Wang YQ, Wang K, Cheng WL, Zhang YQ. Global burden of chronic obstructive pulmonary disease attributable to ambient ozone in 204 countries and territories during 1990-2019. Environ Sci Pollut Res Int 2022;29(6):9293 – 305. http://dx.doi.org/10.1007/s11356-021-16233-y.
3. Zhang Y, Tian QQ, Feng XY, Hu WD, Ma P, Xin JY, et al. Modification effects of ambient temperature on ozone-mortality relationships in Chengdu, China. Environ Sci Pollut Res Int 2022;29 (48):73011 – 9. http://dx.doi.org/10.1007/s11356-022-20843-5.
4. Chen C, Liu J, Shi WY, Li TT, Shi XM. Temperature-modified acute effects of ozone on human mortality—Beijing municipality, Tianjin municipality, Hebei province, and surrounding Areas, China, 2013-2018. China CDC Wkly 2021;3(45):964 – 8. http://dx.doi.org/10.46234/ccdcw2021.234.
5. Cui LL, Conway GA, Jin L, Zhou JW, Zhang J, Li XW, et al. Increase in medical emergency calls and calls for central nervous system symptoms during a severe air pollution event, January 2013, Jinan City, China. Epidemiology 2017;28 Suppl 1:S67-73. http://dx.doi.org/10.1097/EDE.0000000000000739.
6. Pintarić S, Zeljković I, Pehnec G, Nesek V, Vrsalović M, Pintarić H. Impact of meteorological parameters and air pollution on emergency department visits for cardiovascular diseases in the city of Zagreb, Croatia. Arh Hig Rada Toksikol 2016;67(3):240 – 6. http://dx.doi.org/10.1515/aiht-2016-67-2770.
7. Ding PH, Wang GS, Guo YL, Chang SC, Wan GH. Urban air pollution and meteorological factors affect emergency department visits of elderly patients with chronic obstructive pulmonary disease in Taiwan. Environ Pollut 2017;224:751 – 8. http://dx.doi.org/10.1016/j.envpol.2016.12.035.
8. Pryor WA, Squadrito GL, Friedman M. A new mechanism for the toxicity of ozone. Toxicol Lett 1995;82-83:287 – 93. http://dx.doi.org/10.1016/0378-4274(95)03563-X.
9. Appenheimer MM, Evans SS. Temperature and adaptive immunity. Handb Clin Neurol 2018;156:397 – 415. http://dx.doi.org/10.1016/B978-0-444-63912-7.00024-2.

SUPPLEMENTARY MATERIAL

Methods

An Overview of Jinan City

Jinan City, the capital of Shandong Province, is situated between 36°01′–37°32′ N latitude and 116°11′–117°44′ E longitude. It spans a total area of 10,244 km^2 and is divided into 10 administrative districts, and the rate of medical emergency calls (MECs) showed minor fluctuations from 2013 to 2019 (Supplementary Table S1)(*1*). The city exhibits a classic temperate monsoon climate characterized by chilly winters, hot summers, and distinct seasonal changes. What's more, Jinan City, renowned as one of China's traditional "furnace cities", experiences severe heat in the summer months. Since 1951, there has been a steady increase in the city's temperature at a rate of 0.24 ℃ per decade, exhibiting an almost linear upward trend (*2*). Notably, the highest recorded temperature was 39.9 ℃ on July 13, 2015. Jinan suffers from substantial air pollution, with a historical PM$_{2.5}$ record peaking at 443 μg/m^3 during the 2013 haze incident (*3*). It serves as a pivotal link between two prominent economic zones, the Beijing-Tianjin-Hebei Regions and the Yangtze River Delta. In recent years, Jinan has undergone swift industrialization and urbanization processes. Almost 40% of Jinan's gross domestic product (GDP) stems from key industries such as power plants, manufacturing, textile and steel production, chemical manufacturing, light industry, and building materials (*3*). Consequently, Jinan City has been identified as one of the top ten cities in China for air pollution, with escalating O$_3$ pollution observed since 2013.

MECs Data Collection

Established in 1956, the Jinan Medical Emergency Center (JMEC) is charged with managing emergency health requests from the population via a "120" hotline available round the clock. JMEC oversees 66 first-aid service stations affiliated with hospitals, providing coverage across all ten administrative districts of Jinan City (Supplementary Table S2). For this research, daily data from JMEC's MECs were gathered for the period spanning May 1 to September 31 for the years 2013–2019.

Upon receipt of a call through the hotline, the physicians on duty promptly register pertinent emergent medical information. This includes the caller's telephone number, the time of the call, the address of either the patient or the accident, and any reported health complaints. These health complaints are then categorized into respective clinical diagnostic descriptors while also inquiring about additional health-related issues. Emergency calls can be divided into two main types: emergency and non-emergency. For the purpose of this study, non-emergency calls — which encompass calls associated with accidents, service types such as transfers, evacuations, equipment rentals, testing, and trauma — were excluded in order to establish a database of MECs.

The Time-Stratified Case-Crossover Model Analysis

The fundamental principle underpinning the time-stratified case-crossover study involves time stratification, wherein the case phase and control phase occur within the same time stratum. Specifically, within a given time stratum, multiple control periods, both preceding and following the case period, are matched according to the same year, month, and weekday (*4*). This design permits an event day to correspond to 3 to 4 control days. For example, if an event day occurs on May 16, 2013 (a Thursday), other Thursdays in May of 2013 would be selected as control days. Furthermore, in consideration of confounding factors, relative humidity (RH) is incorporated into the regression model as a covariate. The fundamental equation for this core model is presented below:

$$Log[E(Y_t)] = \alpha + \beta_1 temperature + \beta_2 O_3 + \beta_3 (temperature + O_3)_t + RH + stratum \tag{1}$$

Where *E(Y)* is the expected number of MECs at time *t*; *t* is event date; α is the intercept; β is vector of regression coefficients; and (*temperature+O₃*)$_t$ is the interaction between temperature and O$_3$ concentration on day *t*; *stratum* is the categorical variable, which is the matching variable of year, month, and week.

Several sensitivity analyses were carried out to evaluate the robustness of the main findings. Under optimal effect periods, the main model was adjusted by incorporating the air pollutants (PM$_{2.5}$, NO$_2$) and meteorological factors (wind speed, pressure), separately.

SUPPLEMENTARY TABLE S1. The information of resident population and MECs rate in Jinan City from 2013 to 2019.

Year	Resident year-end population	MECs volume	MECs rate (%)
2013	6,999,000	35,380	0.51
2014	7,067,000	38,547	0.54
2015	7,132,000	41,453	0.58
2016	7,233,000	34,459	0.48
2017	7,321,000	38,373	0.52
2018	7,460,400	37,573	0.50
2019	7,613,000	42,571	0.56

Abbreviation: MECs=medical emergency calls.

SUPPLEMENTARY TABLE S2. The information of JMECS.

S.N.	Name of JMECS	District/country	Area type
1	Shanghe County People's Hospital	Shanghe	Rural
2	Shanghe County Chinese Medicine Hospital	Shanghe	Rural
3	Shanghe County Puji Hospital	Shanghe	Rural
4	Jiyang District People's Hospital	Jiyang	Rural
5	Jiyang District Chinese Medicine Hospital	Jiyang	Rural
6	Zhangqiu District People's Hospital	Zhangqiu	Rural
7	Zhangqiu District Chinese Medicine Hospital	Zhangqiu	Rural
8	Zhangqiu District Wenzu Health Centre	Zhangqiu	Rural
9	Zhangqiu District Shuizhai Health Centre	Zhangqiu	Rural
10	The Second Hospital of Shandong University	Tianqiao	Urban
11	Tianqiao District Daqiao Township Health Centre	Tianqiao	Urban
12	Provincial Third Hospital	Tianqiao	Urban
13	Provincial Third Hospital Xincheng Campus	Tianqiao	Urban
14	Jinan Hebei Fourth Hospitals	Tianqiao	Urban
15	Jinan Central Hospital Huashan Station	Tianqiao	Urban
16	Jinan Fourth People's Hospital	Tianqiao	Urban
17	Huanghe Hospital	Tianqiao	Urban
18	Jinan Central Hospital Gangou Station	Licheng	Urban
19	People's Liberation Army Hospital 960	Licheng	Urban
20	Jinan Third People's Hospital	Licheng	Urban
21	Jinan Third People's Hospital Tangwang	Licheng	Urban
22	Jinan Seventh People's Hospital	Licheng	Urban
23	Jinan Jigang Hospital	Licheng	Urban
24	The Second Hospital of SU	Licheng	Urban
25	Shandong University School Hospital	Licheng	Urban
26	Licheng District People's Hospital	Licheng	Urban
27	Jinan Puxian Hospital	Licheng	Urban
28	Jinan Lingang Hospital	Licheng	Urban
29	Jinan Tangye Hospital	Licheng	Urban
30	Jinan MECS	Lixia	Urban
31	Jinan Central Hospital Yajuyuan Station	Lixia	Urban

Continued

S.N.	Name of JMECS	District/country	Area type
32	Jinan Central Hospital Qilu Garden Station	Lixia	Urban
33	Thousand Buddha Mountain Hospital	Lixia	Urban
34	Jinan Hospital	Lixia	Urban
35	Provincial Hospital East Campus	Lixia	Urban
36	Qilu Hospital	Lixia	Urban
37	Jinan First People's Hospital	Lixia	Urban
38	Shandong Chinese Medicine Hospital East Campus	Lixia	Urban
39	Lixia District People's Hospital	Lixia	Urban
40	Lixia District Third PH	Lixia	Urban
41	Jinan Puji Hospital	Lixia	Urban
42	Jinan Fifth People's Hospital	Huaiyin	Urban
43	Jinan 106 Hospital	Huaiyin	Urban
44	Jinan Fifth People's Hospital Dajin Station	Huaiyin	Urban
45	Huaiyin District People's Hospital	Huaiyin	Urban
46	Shandong Hand-Foot Surgery Hospital	Huaiyin	Urban
47	Provincial Hospital West Campus	Huaiyin	Urban
48	Jinan 106 Hospital West Station	Huaiyin	Urban
49	Jinan Zhongde Orthopaedic Hospital	Huaiyin	Urban
50	Jinan Maternal and Child Health Centre	Shizhong	Urban
51	Jinan Chinese Medicine Hospital	Shizhong	Urban
52	Jinan MECS Second Station	Shizhong	Urban
53	Shizhong District People's Hospital	Shizhong	Urban
54	Shandong Provincial Police General Hospital	Shizhong	Urban
55	The Second Affiliated Hospital of Shandong University of Traditional Chinese Medicine	Shizhong	Urban
56	Jinan Santa Maria Hospital	Shizhong	Urban
57	Jinan Central Hospital Shandong Power Station	Shizhong	Urban
58	Jinan Microsurgery Hospital	Shizhong	Urban
59	Changqing District People's Hospital	Changqing	Rural
60	Changqing District Chinese Medicine Hospital	Changqing	Rural
61	Changqing District Zhangxia Station	Changqing	Rural
62	Changqing District Xiaoli Station	Changqing	Rural
63	Pingyin County People's Hospital	Pingyin	Rural
64	Pingyin Traditional Chinese Medicine Hospital	Pingyin	Rural
65	Pingyin County Dong'a Town Centre Health Centre	Pingyin	Rural
66	Pingyin County Xiaozhi Township Health Centre	Pingyin	Rural

Abbreviation: S.N.=serial number; JMECS=Jinan Medical Emergency Centre Station; MECs=medical emergency calls.

RESULTS

Correlation Analysis

The chronologically displayed diagram depicting the correlations among temperature, O_3 concentration, and MECs demonstrates a high degree of consistency, suggesting potential relationships (Supplementary Figure S1). Furthermore, temperature demonstrates a positive correlation with wind speed and a negative correlation with

SUPPLEMENTARY TABLE S3. Correlation coefficient (r_s value) between meteorological factors and air pollutants in Jinan City, from May to September 2013–2019.

Variables	RH (%)	WS (m/s)	PM$_{2.5}$	PM$_{10}$	NO$_2$	SO$_2$	CO	O$_3$
Pressure (hPa)	−0.13*	−0.19*	0.04*	0.12*	0.10*	0.10*	−0.13*	−0.15*
Temperature (℃)	−0.29*	0.10*	−0.01*	−0.01*	−0.25*	−0.09*	−0.12*	0.63*
RH (%)		−0.38*	0.06*	−0.29*	−0.04*	−0.13*	0.16*	−0.56*
WS (m/s)			0.08*	0.09*	−0.36*	0.08*	−0.18*	0.04*
PM$_{2.5}$				0.87*	0.54*	0.66*	0.68*	0.14*
PM$_{10}$					0.57*	0.65*	0.55*	0.25*
NO$_2$						0.63*	0.62*	−0.02*
SO$_2$							0.62*	0.02*
CO								−0.07*

Abbreviation: RH=relative humidity; WS=wind speed.
* $P<0.05$.
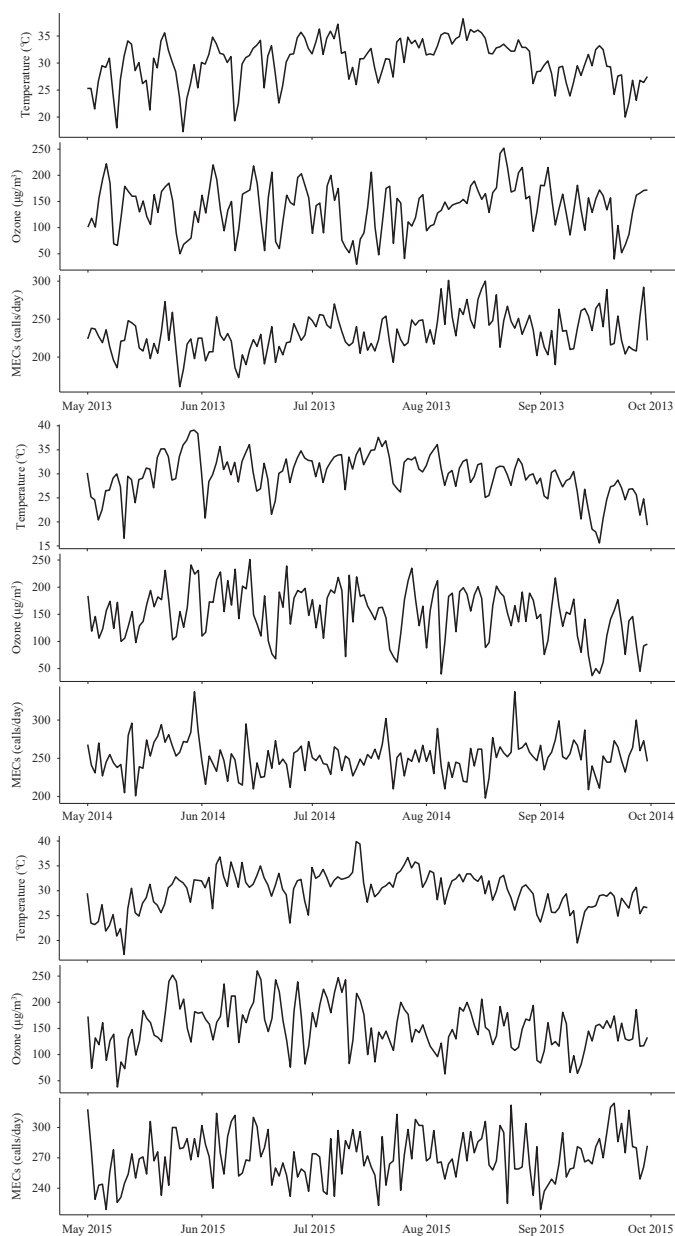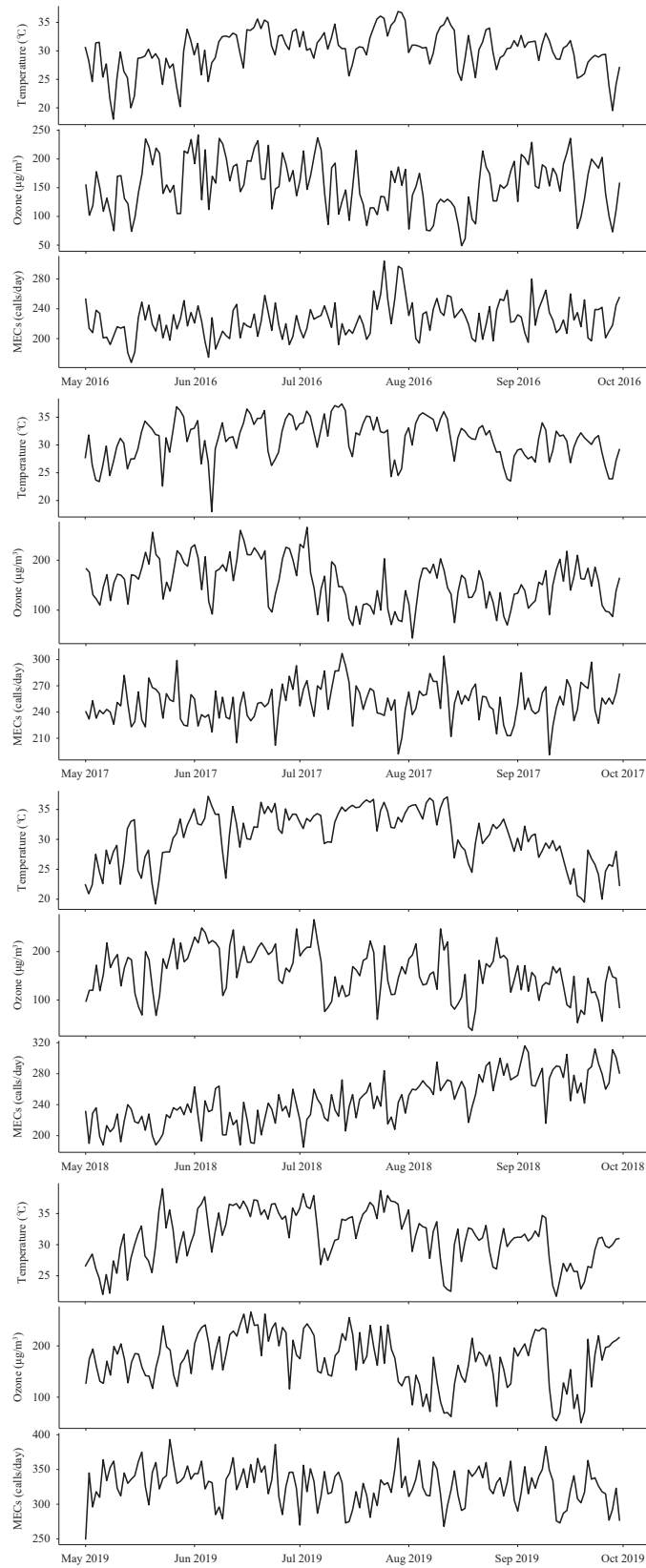
SUPPLEMENTARY FIGURE S1. Time sequence diagram of temperature, O₃ concentration, and MECs in Jinan, from May to September 2013–2019.
Abbreviation: MECs=medical emergency calls; May=May; Jun=June; Jul=July; Aug=August; Sep=September; Oct=October.
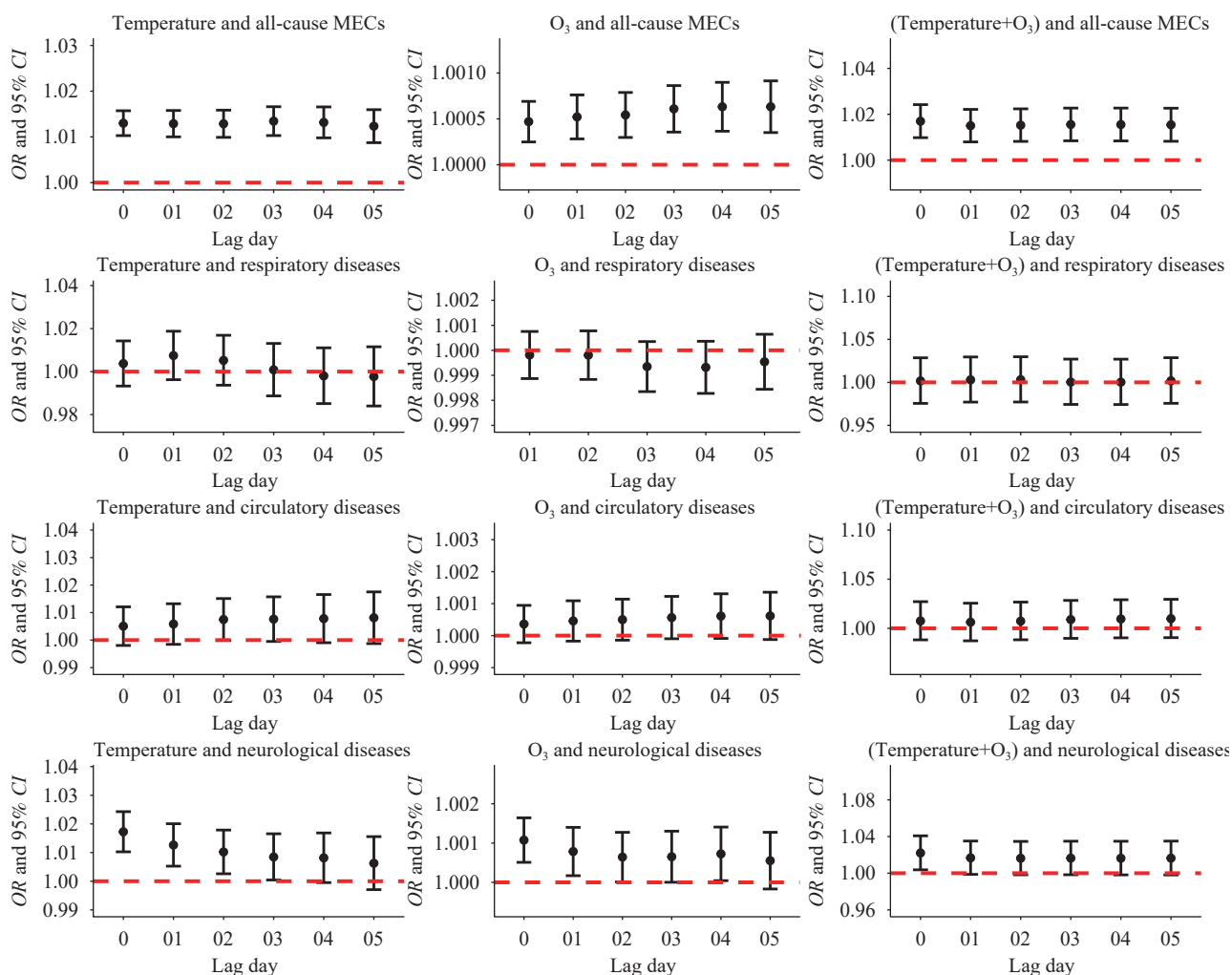
SUPPLEMENTARY FIGURE S2. The cumulative lag effect of temperature, O_3, and temperature combined with O_3 on the all-cause MECs and MECs for different system diseases in the warm season of Jinan, 2013–2019.
Note: The variable "Temperature+O_3" in this study represents the combined impact of high temperature and ozone pollution.
Abbreviation: *OR*=odds ratio; *CI*=confidence interval; MECs=medical emergency calls.

relative humidity and other atmospheric pollutants. O_3 concentration is positively correlated with wind speed, $PM_{2.5}$, PM_{10}, and SO_2, but it is negatively correlated with relative humidity, NO_2, and CO (Supplementary Table S3).

Effects of Temperature and Ozone Pollution on Medical Emergency Calls

Supplementary Figure S2 illustrates the results of the cumulative lag effect analysis for temperature, O_3 pollution, and their combination. Our analysis revealed statistically significant impacts of temperature, O_3 pollution, and the combination of temperature and O_3 pollution on all-cause mortality and morbidity events. Notably, the most pronounced effects were observed at Lag03, Lag04, and Lag0 for temperature, O_3 pollution, and the combination, respectively. Furthermore, our investigation uncovered that the cumulative lag effects of temperature and O_3 pollution on mortality and morbidity events related to respiratory, circulatory, and neurological diseases were consistent with the findings from the single-day lag effect analysis.

Sensitivity Analysis

This study employs a sensitivity analysis to assess the robustness of the estimated effect value by the master model, taking into account the presence of additional air pollutants and meteorological factors such as $PM_{2.5}$, NO_2, wind speed, pressure, and a combined category of all these factors, throughout the perpetual duration of optimum effect.
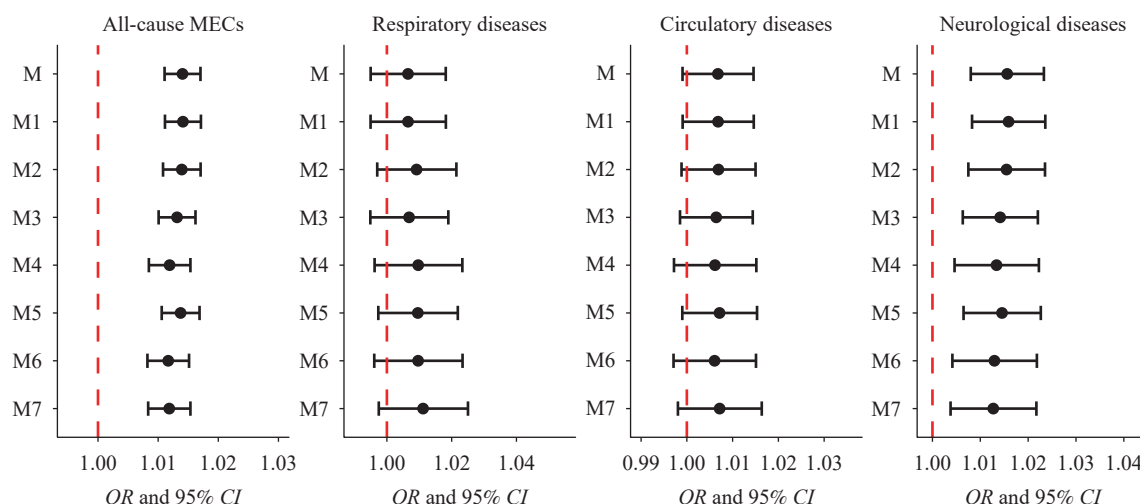
SUPPLEMENTARY FIGURE S3. The effects of temperature combined with O_3 pollution on MECs of different system diseases after adding other factors.

Note: M refers to the master model, M1 represents the adjustment of $PM_{2.5}$, M2 represents the adjustment of NO_2, M3 represents the adjustment of wind speed, M4 represents the adjustment of pressure, M5 represents the adjustment of $PM_{2.5}$ and NO_2, M6 represents the adjustment of wind speed and pressure, and M7 represents the adjustment of $PM_{2.5}$, NO_2, wind speed, and pressure.

Abbreviation: OR=odds ratio; CI=confidence interval; MECs=medical emergency calls.

Supplementary Figure S3 displays the estimated effect value and the corresponding confidence interval of temperature combined with O_3 pollution on various health outcomes (including all-cause, respiratory diseases, circulatory diseases, and neurological diseases). Notably, these estimates remain mostly unchanged when relevant parameters are altered. These findings demonstrate the appropriateness of the chosen model parameters in this study and validate the robustness of the model fitting results.

REFERENCES

1. Jinan Municipal Bureau of Statistics. Jinan statistical yearbook. Beijing: Science Press. 2014–2020. http://jntj.jinan.gov.cn/col/col27523/index.html. (In Chinese).
2. Hu G, Song H. Analysis of air-temperature variation trend and abrupt change in Jinan based on Mann-Kendall test. J Univ Jinan Sci Technol 2012;26(1): 96 – 101. http://dx.doi.org/10.3969/j.issn.1671-3559.2012.01.021. (In Chinese).
3. Cui LL, Zhang J, Zhang J, Zhou JW, Zhang Y, Li TT. Acute respiratory and cardiovascular health effects of an air pollution event, January 2013, Jinan, China. Public Health 2016;131:99 – 102. http://dx.doi.org/10.1016/j.puhe.2015.11.003.
4. Janes H, Sheppard L, Lumley T. Case-crossover analyses of air pollution exposure data: referent selection strategies and their implications for bias. Epidemiology 2005;16(6):717 – 26. http://dx.doi.org/10.1097/01.ede.0000181315.18836.9d.

Preplanned Studies

Associations Between Air Temperature and Daily Varicella Cases — Jinan City, Shandong Province, China, 2019–2021

Guijie Luan[1,2]; Yuehua Hu[1]; Meng Chen[2]; Meiying You[1]; Chengdong Xu[3]; Dapeng Yin[4]; Jianjun Liu[1]; Hongyan Yao[1,#]

Summary

What is already known about this topic?

The impact of air temperature on varicella has been studied, but there is limited research exploring its effect on varicella by gender and age group.

What is added by this report?

We conducted a time series analysis to examine the differential effects of air temperature on varicella infection across different demographic groups. Our findings indicate that lower temperatures have a more pronounced influence on varicella incidence among males and children compared to females and adults.

What are the implications for public health practice?

These findings can assist in identifying populations that are vulnerable to temperature-related varicella and in guiding the implementation of effective measures for varicella control.

Varicella, an acute respiratory infectious disease primarily affecting children, has been shown in several studies to be influenced by air temperature (*1–2*). However, little research has been conducted on the effects of air temperature on varicella incidence based on gender and age groups. This study aims to examine the association between air temperature and varicella and identify any group-specific differences in temperature-related risk. A distributed lag non-linear model (DLNM) was utilized to assess the impact of air temperature on varicella incidence in Jinan City, Shandong Province from 2019 to 2021. Our findings indicate that both gender and age exhibit diverse impacts of higher and lower temperatures on varicella incidence. Lower temperatures have a greater effect on varicella incidence in males compared to females, particularly within 1–4 days of exposure. The relative impacts of higher and lower temperatures on varicella incidence in adults only persist for around 2 days, whereas lower temperatures have a significantly higher and longer-lasting impact on varicella incidence in children, lasting up to 10 days. These results provide

valuable insights for future risk assessments of temperature-related infectious diseases and emphasize the importance of implementing targeted public health measures for vulnerable populations in relation to air temperature.

Meteorological factors, particularly air temperature, are known to influence the incidence of varicella (*1–5*). However, there is limited research on the impact of low temperature on varicella. Previous studies have suggested that relative humidity may reduce the risk of varicella incidence (*3*). The correlation between other meteorological factors such as rainfall and wind speed and varicella incidence remains unclear. Therefore, in this study, we aimed to control for confounding factors, including relative humidity, rainfall, and wind speed (*4–5*). We collected daily reported varicella cases from the Chinese infectious diseases reporting system in Jinan City from 2019 to 2021. The data were categorized by gender and age, and we identified a total of 6,528 male and 5,182 female varicella cases. Varicella cases were further classified as either adult (age ≥18 years) or child (age <18 years) (*6*), with 7,266 child cases and 4,444 adult cases reported. Additionally, we obtained daily mean temperature, relative humidity, rainfall, and windspeed data for the same period from the National Centers for Environmental Information (NCEI) website (https://www.ncei.noaa.gov/).

We employed a DLNM with a quasi-Poisson distribution to evaluate the influence of air temperature on varicella. To capture non-linear relationships between air temperature and varicella incidence, we used a natural cubic spline with 7 degrees of freedom (df). Lag effects, relative humidity, rainfall, and windspeed were modeled using 3 df each. Indicator variables were included for days of the week and holidays. We focused on a lag of 14 days to analyze the cumulative effect, lag effect, and incubation period of varicella. Specific details of the model parameters and sensitivity analyses can be found in the supplementary materials. The analysis was conducted using R software (version 4.2.2; R Foundation for

Statistical Computing, Auckland, New Zealand), utilizing the DLNM package.

The average air temperature was 13.3 ℃, with a range of −13.5 ℃ to 30.4 ℃ for air temperature, 19.7% to 97.8% for relative humidity, 0 mm to 170.6 mm for rainfall, and 2.2 m/s to 15.9 m/s for windspeed (Supplementary Table S1, available in https://weekly.chinacdc.cn/). Both higher and lower air temperatures were found to increase the risk of varicella (Figure 1). The risk of varicella gradually increased when the air temperature fell outside a certain range. The maximum relative risk (RR) for higher temperatures was 1.15 [95% confidence interval (*CI*): 1.05, 1.26] at lag 0 days, while the maximum RR for lower temperatures was 1.09 (95% *CI*: 0.84, 1.41)
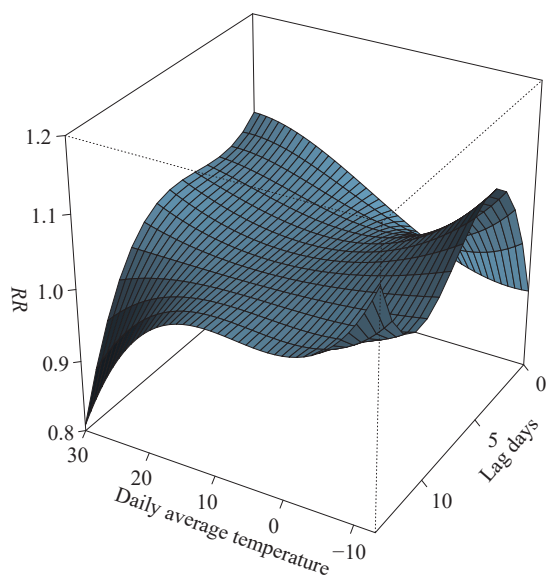
at lag 14 days. The impact of lower air temperature on varicella lasted approximately 10 days, whereas the impact of higher air temperature typically only lasted around 2 days.

The influence of higher air temperature on both male and female varicella infections was found to be greater when there was a lag of 0–3 days (Figure 2). Conversely, lower air temperature had a stronger effect on varicella in males compared to females, particularly with a lag of 1–4 days. The highest RR of lower air temperature on varicella in males was 1.25 (95% *CI*: 0.79, 1.92) at a lag of 3 days, while in females it was 1.20 (95% *CI*: 0.82, 1.68) at a lag of 5 days (Figure 2).

Figure 3 illustrates that the effect of lower air temperatures on varicella in children is significantly higher compared to adults and persists for approximately 10 days. In contrast, the impact on adults only lasts for about 2 days. The maximum RR of lower air temperature on varicella in children is 1.33 (95% *CI*: 0.78, 2.30) at a lag of 4 days, while in adults it is 1.16 (95% *CI*: 0.87, 1.54) at a lag of 0 days. Additionally, the effect of higher air temperatures on varicella in both adults and children only lasts for approximately 2 days.

DISCUSSION

This study explores the relationship between air temperature and varicella incidence in Jinan from 2019 to 2021, with a focus on gender and age differences. We observed that lower air temperatures had a greater impact on varicella morbidity compared to higher air temperatures. Furthermore, there were differences in how air temperature affected varicella based on gender and age, with males and children being more vulnerable to temperature-related risks. These findings emphasize the need for targeted varicella prevention

FIGURE 1. The 3D plot of the daily average temperature on varicella from 2019 to 2021 in Jinan City, Shandong Province, China.
Abbreviation: *RR*=relative risk.

FIGURE 2. Exposure-response relationship of daily average temperature on varicella between (A) male and (B) female from 2019 to 2021 in Jinan City, Shandong Province, China.
Abbreviation: *RR*=relative risk.
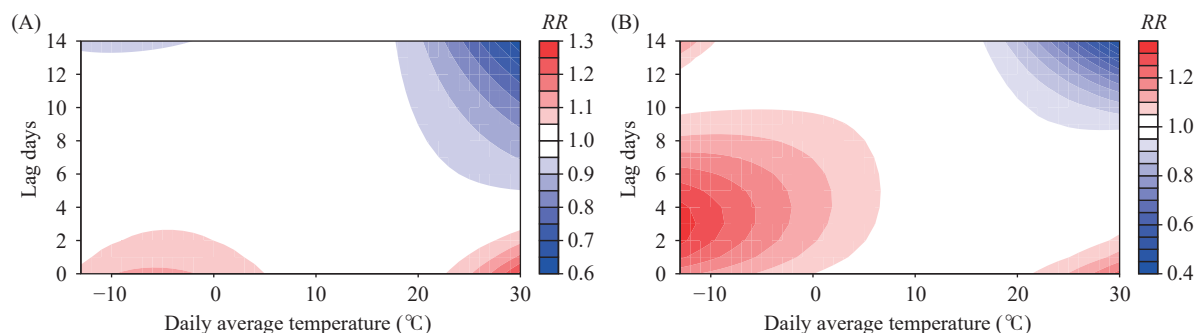
FIGURE 3. Exposure-response relationship of daily average temperature on varicella between (A) adults and (B) children of 2019 to 2021 in Jinan City, Shandong Province, China.
Abbreviation: *RR*=relative risk.

strategies for vulnerable populations based on temperature variations. For instance, a study conducted in Guangzhou found that the relative risk was highest at 1.11 (95% *CI*: 1.07, 1.16) with a 21-day lag when the mean temperature was 31.8 ℃ (*2*). On the other hand, a study in Lu'an City, Anhui Province (in eastern China) identified that the maximum single-day lag effects of varicella were 1.29 (95% *CI*: 1.20, 1.38) at a 16-day lag when the mean temperature was –5.8 ℃ (*5*). Previous studies have not consistently reported gender and age differences in temperature-related morbidity risk. Our subgroup analysis revealed that males and children were high-risk groups for temperature-related varicella, particularly in cases of lower air temperature.

There may also be differences in responses to higher air temperatures between males and females. This could be due to males engaging in more outdoor activities and being more susceptible to the impacts of higher air temperatures, while females tend to take protective measures during periods of high temperature. The greater impact of lower air temperature on varicella in males may be related to physiological factors such as body shape and hormonal influences. A study by the University of Cambridge in the UK demonstrated that in response to harsh cold environments, blood vessels in the hands and feet naturally contract to protect vital organs like the heart from inadequate blood supply (*7*). Although both males and females experience cold, females generally exhibit greater sensitivity to temperature, leading them to respond more quickly to temperature changes. Some studies have indicated an annual increase in reported varicella cases among older age groups (*8*).

Ambient temperature can directly impact biochemical reactions within the body and have direct or indirect effects on various systems. The impact of higher or lower temperatures on varicella in adults is relatively small due to their better adaptability to temperature changes. Adults tend to take effective protective measures, such as adjusting clothing and utilizing air conditioning, to mitigate the potential damage caused by temperature changes. Additionally, ambient temperature can also influence the function of the body's immune system, potentially reducing resistance to viruses and bacteria to a certain extent. However, children's physical development is not fully mature, and their regulatory mechanisms may not meet the requirements when faced with extreme temperatures (*9*).

This study has a few limitations. First, we acknowledge the presence of ecological fallacy, as it was not possible to measure individual exposure accurately. Second, limited studies have suggested that air pollution may also contribute to increased varicella incidence (*10*), which should be considered and adjusted for in future research.

In summary, we found that there are gender and age variations in the relationship between air temperature and varicella. These findings can contribute to the identification of vulnerable populations at risk of temperature-related varicella and inform the development of effective varicella control strategies.

Conflicts of interest: No conflicts of interest.

Corresponding author: Hongyan Yao, yaohy@chinacdc.cn.

1 Chinese Center for Disease Control and Prevention, Beijing, China;
2 Institute for Immunization management, Shandong Center for

Disease Control and Prevention, Jinan City, Shandong Province, China; [3] State Key Laboratory of Resources and Environmental Information System, Institute of Geographic Sciences and Natural Resources Research, Chinese Academy of Sciences, Beijing, China; [4] Hainan Provincial Center for Disease Control and Prevention, Haikou City, Hainan Province, China.

REFERENCES

1. Li Y, Li J, Zhu Z, Zeng W, Zhu Q, Rong Z, et al. Exposure-response relationship between temperature, relative humidity, and varicella: a multicity study in South China. Environ Sci Pollut Res Int 2023;30(3):7594 – 7604. http://dx.doi.org/10.1007/s11356-022-22711-8.
2. Lu JY, Zhang ZB, He Q, Ma XW, Yang ZC. Association between climatic factors and varicella incidence in Guangzhou, Southern China, 2006-2018. Sci Total Environ 2020;728:138777. http://dx.doi.org/10.1016/j.scitotenv.2020.138777.
3. Yang Y, Geng X, Liu X, Wang W, Zhang J. Association between the incidence of varicella and meteorological conditions in Jinan, Eastern China, 2012-2014. BMC Infect Dis 2016;16:179. http://dx.doi.org/10.1186/s12879-016-1507-1.
4. Hervás D, Hervás-Masip J, Nicolau A, Reina J, Hervás JA. Solar radiation and water vapor pressure to forecast chickenpox epidemics. Eur J Clin Microbiol Infect Dis 2015;34:439 – 46. http://dx.doi.org/10.1007/s10096-014-2243-3.
5. Zhang T, Qin W, Nie T, Zhang D, Wu X. Effects of meteorological factors on the incidence of varicella in Lu'an, Eastern China, 2015–2020. Environ Sci Pollut Res Int 2023;30:10052 – 62.
6. Mama RS. Needs, rights, and the human family: the practicality of the Convention on the Rights of the Child. Child Welfare 2010;89:177 – 89.
7. Bain AR, Ainslie PN, Bammert TD, Hijmans JG, Sekhon M, Hoiland RL, et al. Passive heat stress reduces circulating endothelial and platelet microparticles. Exp Physiol 2017;102:663 – 9.
8. Fu J, Jiang C, Wang J, Zhao F, Ma T, Shi R, et al. Epidemiology of varicella in Haidian district, Beijing, China-2007–2015. Vaccine 2017;35:2365 – 71.
9. Leyk D, Hoitz J, Becker C, Glitz KJ, Nestler K, Piekarski C. Health Risks and Interventions in Exertional Heat Stress. Dtsch Arztebl Int 2019;116:537 – 44.
10. Wang Z, Li X, Hu P, Li S, Guan J, Wang B, et al. Influence of air pollutants on varicella among adults. Sci Rep 2021;11(1):21020. http://dx.doi.org/10.1038/s41598-021-00507-z.

SUPPLEMENTARY MATERIAL

Model Parameters

The formula is shown below (1):

$$Yt \sim QuasiPoisson(\mu t)$$

$$\log(\mu t) = \alpha + NS(Time, T \times 7) + NS(Humidity, 3) + NS(Rainfall, 3) + NS(Windspeed, 3) + \gamma Dow + \eta Holiday + \beta Temperature$$

In the formula, the variable Yt represents the daily number of varicella cases at a given time t. The intercept is represented by α, and there are coefficients γ, η, and β. Time is a time trend variable, and a natural cubic spline curve was used to model it. We controlled for the long-term trend and seasonality effects using NS (Time). We also controlled for the effects of relative humidity using NS (Humidity), the effects of rainfall using NS (Rainfall), and the effects of windspeed using NS (Windspeed). Additionally, Dow represents the day of the week, indicating the presence of a weekend effect, and Holiday represents public holidays, indicating the presence of a holiday effect.

This study aimed to assess the relationship between daily average temperature and daily varicella incidence. Previous studies have shown a decreased risk of varicella with higher relative humidity (2–3). However, the correlation between meteorological factors and varicella incidence, particularly rainfall and wind speed, remains unclear. Furthermore, the impact of rainfall on varicella incidence has shown significant variation (4–5). Therefore, this study sought to account for potential confounding factors, including relative humidity, rainfall, and wind speed, in order to obtain accurate research results.

SUPPLEMENTARY TABLE S1. Descriptive data on daily varicella incidence and weather conditions in Jinan City, Shandong Province, China, 2019–2021.

Variables	Min	Median	Max	Mean	SD
Mean temperature (℃)	−13.5	13.8	30.4	13.3	10.0
Relative humidity (%)	19.7	58.8	97.8	59.3	17.2
Rainfall (mm)	0	0	170.6	2.2	8.9
Windspeed (m/s)	2.2	5.5	15.9	5.8	1.9
Cases					
Total	0	9	50	10.7	7.7
Male	0	5	26	6	4.7
Female	0	4	26	4.7	3.7
Child	0	5	31	6.6	5.6
Adult	0	3	19	4.1	3.2

Abbreviation: Min=minimum; Max=maximum; SD=standard deviation.
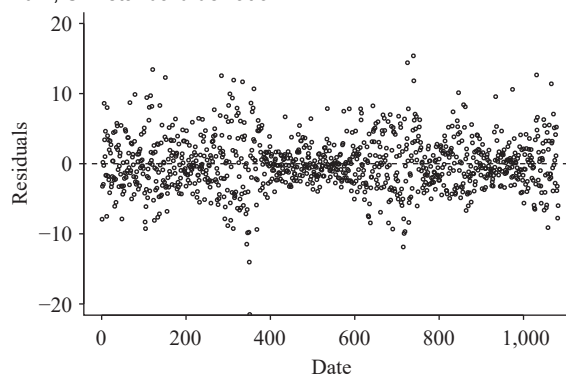
SUPPLEMENTARY FIGURE S1. Sensitivity analyses of the distributed lag non-linear model from 2019 to 2021 in Jinan City, Shandong Province, China.
Notes: Residuals were symmetrically distributed above and below 0. By changing parameters such as the maximum lag and degrees of freedom (df) of long-term trends, it was found that the model fitting results showed no significant fluctuations, indicating the overall stability of the model. It was proven that our model was stable and could be applied.

REFERENCES

1. Gasparrini A. Distributed lag linear and non-linear models in R: the package dlnm. J Stat Softw 2011;43:1-20. https://pubmed.ncbi.nlm.nih.gov/22003319/.
2. Chan JY, Tian LW, Kwan Y, Chan W, Leung C. Hospitalizations for varicella in children and adolescents in a referral hospital in Hong Kong, 2004 to 2008: a time series study. BMC Public Health 2011;11:366. http://dx.doi.org/10.1186/1471-2458-11-366.
3. Yang YQ, Geng XY, Liu XX, Wang WR, Zhang J. Association between the incidence of varicella and meteorological conditions in Jinan, eastern China, 2012-2014. BMC Infect Dis 2016;16:179. http://dx.doi.org/10.1186/s12879-016-1507-1.
4. Hervás D, Hervás-Masip J, Nicolau A, Reina J, Hervás JA. Solar radiation and water vapor pressure to forecast chickenpox epidemics. Eur J Clin Microbiol Infect Dis 2015;34(3):439 – 46. http://dx.doi.org/10.1007/s10096-014-2243-3.
5. Harigane K, Sumi A, Mise K, Kobayashi N. The role of temperature in reported chickenpox cases from 2000 to 2011 in Japan. Epidemiol Infect 2015;143(12):2666 – 78. http://dx.doi.org/10.1017/S095026881400363X.

Preplanned Studies

Disease and Economic Burden of Kashin-Beck Disease — China, 2021

Silu Cui[1,&]; Wenjun Que[2,&]; Zhe Jiao[1]; Qing Deng[1]; Xufeng Zhang[1]; Yanhong Cao[1]; Ning Liu[1]; Ailin Li[2]; Alphonse Sowanou[2]; Zhe Li[2]; Tuo Wang[2]; Yang Li[2]; Jun Yu[1,#]; Junrui Pei[2,#]

Summary

What is already known about this topic?

Kashin-Beck disease (KBD) is a chronic and degenerative osteoarthropathy characterized by cartilage degeneration. It is an endemic disease that is highly prevalent among the Chinese population and poses a significant health risk.

What is added by this report?

This is the first national report on the economic burden of KBD in China. According to the data from 2021, KBD has caused significant disease and economic burdens. The most substantial reduction in healthy life expectancy was observed among patients with degree II severity and those aged 60 years and older, resulting in a total indirect economic burden of 112.74 million Chinese Yuan (CNY).

What are the implications for public health practice?

The results of this study will contribute to informing the development of tailored prevention and control strategies by the government. These strategies will include targeted policies and recommendations for appropriate healthcare and financial subsidies, which will be based on the demographic characteristics of the endemic areas.

Kashin-Beck disease (KBD) is a chronic, endemic osteoarthritic disease that primarily affects children and adolescents. Its etiology remains uncertain. Mild cases of KBD result in thickening of bones and joints, while severe cases lead to joint deformity and permanent disability (*1–2*).

During the 1960s and 1980s, KBD became highly prevalent in China, with X-ray detection rates of 70% to 80% in the most affected areas (*3*). Thanks to decades of prevention and control efforts, the disease's prevalence in the country has significantly decreased, and no new cases have been reported among children. However, there are still over 170,000 existing KBD patients (*4*).

The objective of this paper is to assess the disease burden and economic impact of KBD in China for the year 2021, focusing on government perspectives. This information will serve as a guideline for formulating and enhancing prevention and control strategies.

The data for this study was obtained from the national surveillance system for KBD and the 2021 national case survey of patients with current endemic disease status. The surveillance data from 2002 to 2021 included information on the incidence and prevalence of KBD in 13 provincial-level administrative divisions (PLADs, including Hebei, Shanxi, Inner Mongolia, Liaoning, Jilin, Heilongjiang, Shandong, Henan, Sichuan, Xizang, Shaanxi, Gansu, and Qinghai). The 2021 national case survey collected basic demographic information on KBD severity, age, gender, and place of residence. The population base for this study was determined by the number of permanent residents in villages located in the endemic disease area.

Since KBD does not typically result in immediate fatality but instead causes long-term disability that significantly impacts the patient's quality of life, this research paper aims to evaluate the health consequences of KBD by quantifying the years lived with disability (YLDs). For this analysis, we calculated the prevalence-based YLDs, as outlined in previous studies (*5*). The formula used for this calculation is provided below:

$$YLDs = P \times DW$$

The variable P represents the number of individuals affected by KBD. DW is a weighting factor that reflects the severity of the disease, ranging from 0 (indicating a healthy individual) to 1 (indicating a deceased individual) (*6*). The clinical characteristics of KBD are similar to other musculoskeletal disorders mentioned in the Global Burden of Disease (GBD) 2019 study. Therefore, the disability weights for KBD were directly adopted from the weights assigned to other musculoskeletal disorders in the GBD, which were 0.117 (degree I), 0.317 (degree II) and 0.581 (degree III).

The indirect economic burden is determined by combining YLDs and the human capital method (HM), using the following formula:

Indirect economic burden = national per capita income in the endemic disease area villages × YLDs × productivity weights.

According to Murray's criteria (7), different productivity weights were assigned to different age groups. For children aged 0–14 years who are not yet participating in the social workforce, the productivity weight coefficient was set at 0. The values for age groups 15–44, 45–59, and 60 years and over were set at 0.75, 0.80, and 0.10, respectively. Data on per capita income in endemic villages in each PLAD were obtained from the 2021 National KBD Surveillance Report.

In 2002, there were marked regional variations in the prevalence of KBD, specifically higher rates of positive X-ray findings in children from the western region, including Qinghai (33.96%) and Xizang (27.8%). Due to the implementation of rigorous national preventive and control measures, the incidence of KBD was effectively controlled by 2018, with the prevalence rate in all PLADs approaching 0 (Figure 1A, B). Moreover, no new cases of KBD were

reported among children in affected villages nationwide in 2019, within the timeframe of the "Special Three-Year Action Program for Endemic Disease Control (2018–2020)" (8). From 2002 to 2021, the number of affected individuals decreased from 819,666 to 171,951, although the number of cases in Inner Mongolia, Heilongjiang, Sichuan, Shaanxi, and Gansu PLADs remains above 20,000 (Figure 1C, D).

This study revealed the YLD rates and YLDs in China to be 21.24 YLD/10,000 and 36,018.33 YLDs, respectively. Figure 2 illustrates the spatial distribution of KBD healthy life loss by PLAD, with the most severe areas of healthy life loss concentrated in the western region and Heilongjiang Province. Sichuan (143.79 YLD/10,000, 5,521.43 YLDs) and Xizang (48.00 YLD/10,000, 1,253.33 YLDs) had YLD rates exceeding 30 YLD/10,000 people (Figure 2).

Based on Murray's criteria for assigning productivity weights to different age groups, this study classified KBD patients into three age groups: 15–44, 45–59, and 60 years and above, which accounted for 4.21%, 36.36%, and 59.43% of the total patients, respectively. Among all patients, 62.88%, 30.21%, and 6.91% were categorized as having first, second, and third degree
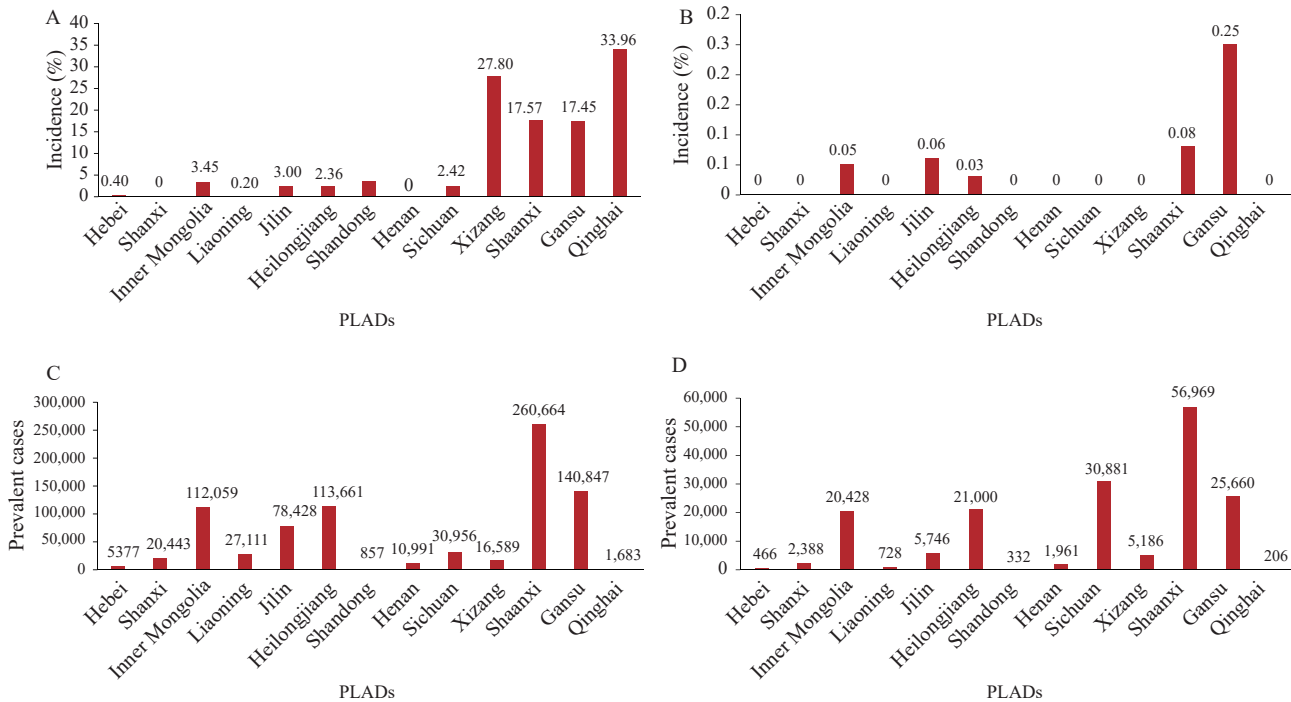
FIGURE 1. Incidence and prevalence of KBD disease by PLAD in China. (A)The incidence of KBD disease by PLAD in China in 2002; (B) The incidence by PLAD in China in 2018; (C) The number of KBD disease patients by PLAD in China in 2002; (D) The number of disease patients by PLAD in China in 2021.
Abbreviation: PLAD=provincial-level administrative division; KBD=Kashin-Beck disease.
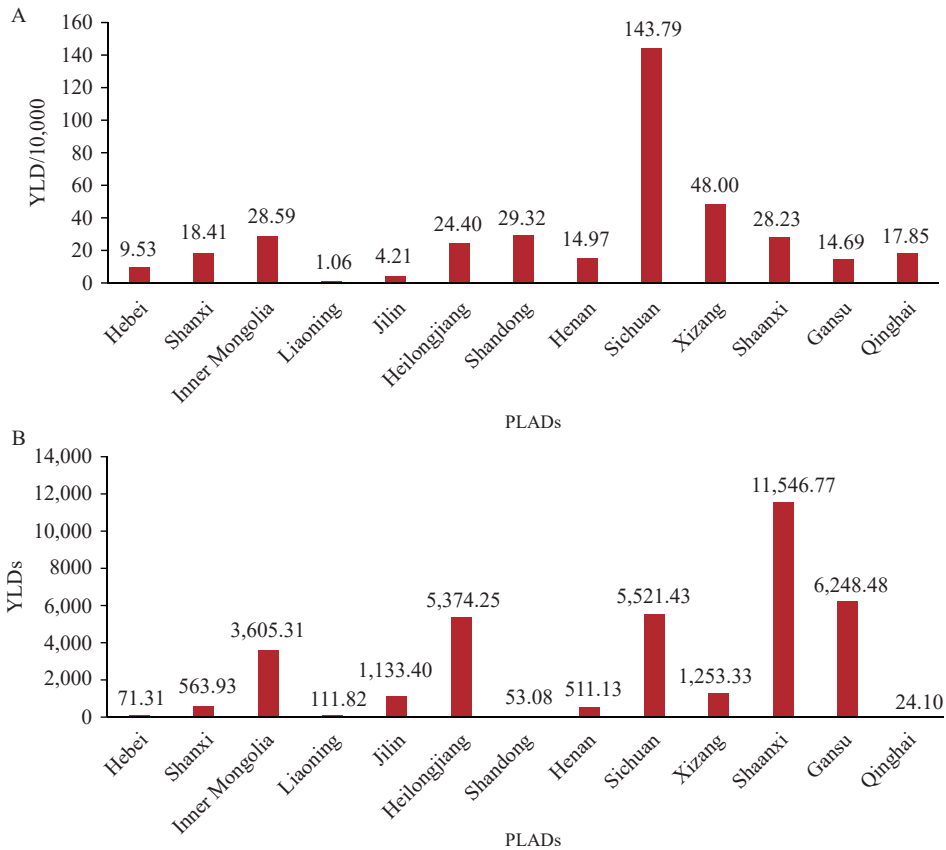
FIGURE 2. YLD rate (A) and YLDs (B) for KBD by PLAD in China, 2021.
Abbreviation: YLDs=years lived with disability; KBD=Kashin-Beck disease; PLAD=provincial-level administrative division.
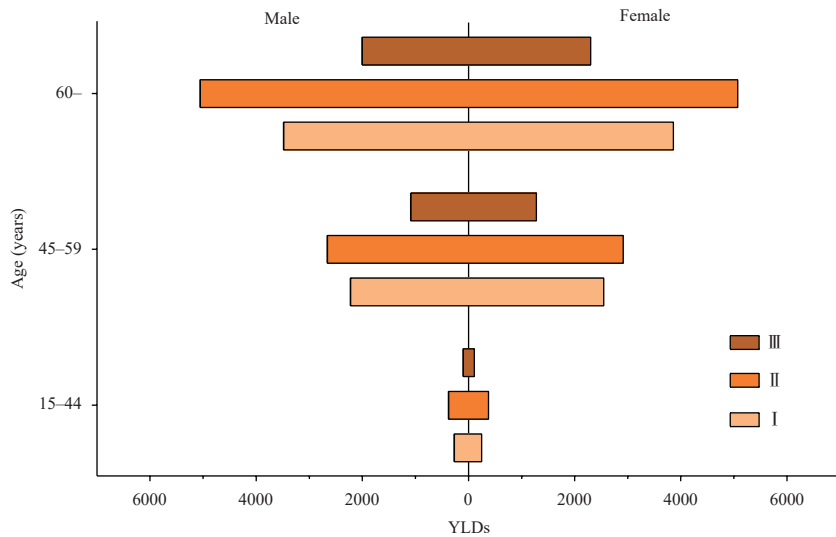
FIGURE 3. Age-sex-specific YLDs among KBD grades in China, 2021.
Abbreviations: YLDs=years lived with disability; KBD=Kashin-Beck disease.

severity respectively.

The results presented in Figure 3 demonstrate a significant increase in YLDs with advancing age ($P<0.05$). Notably, patients with degree II severity and those aged 60 years and above accounted for the largest proportions, with approximately 16,468 and 21,794 YLDs respectively. Additionally, no statistically significant difference in YLDs by gender was observed

TABLE 1. Indirect economic burden of KBD by PLAD in China, 2021.

| PLAD | Indirect economic burden (10,000 CNY) | | | |
| | Age group (years) | | | Total |
	15–44	45–59	60 and above	
Hebei	0.24	4.82	2.59	7.65 (0.07%)
Shanxi	0.62	37.60	26.35	64.57 (0.57%)
Inner Mongolia	115.82	1646.50	96.80	1859.13 (16.49%)
Liaoning	0.00	9.36	14.16	23.52 (0.21%)
Jilin	7.78	185.69	93.31	286.78 (2.54%)
Heilongjiang	51.65	1709.27	270.12	2031.04 (18.02%)
Shandong	0.24	8.43	4.34	13.02 (0.12%)
Henan	1.86	57.16	18.45	77.46 (0.69%)
Sichuan	383.19	1175.41	379.69	1938.29 (17.19%)
Xizang	130.25	108.99	13.13	252.37 (2.24%)
Shaanxi	71.46	2448.08	762.12	3281.66 (29.11%)
Gansu	61.23	1157.37	209.82	1428.43 (12.67%)
Qinghai	2.10	6.79	0.86	9.74 (0.09%)
Total	826.43	8555.47	1891.75	11273.65

Abbreviation: KBD=Kashin-Beck disease; PLAD=provincial-level administrative division; CNY=Chinese Yuan.

across all age categories ($P>0.05$).

According to Table 1, a total of 171,951 patients diagnosed with KBD were included in this analysis of indirect economic costs. The indirect economic burden of KBD in China in 2021 was estimated to be 112.74 million Chinese Yuan (CNY), equivalent to 655.63 CNY per capita per year. PLADs with particularly high indirect economic burdens include Inner Mongolia (18.59 million CNY, 16.49%), Heilongjiang (20.31 million CNY, 18.02%), Sichuan (19.38 million CNY, 17.19%), Shaanxi (32.82 million CNY, 29.11%), and Gansu (14.28 million CNY, 12.67%) (Table 1).

DISCUSSION

This study utilized the YLD indicator to estimate the reduction in healthy life expectancy caused by KBD across 13 Chinese PLADs in 2021. Furthermore, for the first time, the YLD indicator was combined with the human capital approach to calculate the indirect economic burden. This integrated approach allows for a more comprehensive assessment of the impact of KBD on both health and the economy.

The findings of this study revealed that despite China's implementation of various preventive and control measures resulting in zero reported cases of KBD in recent years, there still exists a population of 171,951 patients. The spatial distribution of KBD's impact on healthy life expectancy by PLAD in 2021

identified the western region (Gansu, Sichuan, Inner Mongolia, and Shaanxi) and the eastern region PLAD (Heilongjiang) as experiencing the most pronounced loss in healthy life expectancy. Analysis of the age and gender distribution of healthy life span loss indicated significant discrepancies in YLDs across different age groups ($P<0.05$), with the highest YLDs in the age group of 60 years and over, followed by those aged 45–59 years. Notably, there were no statistically significant gender disparities in YLDs across different disease levels ($P>0.05$), consistent with a previous study conducted in Bin County, Shaanxi Province (9).

The total indirect economic burden in 2021 amounted to 112.74 million CNY, with a per capita burden of 655.63 CNY per year. Inner Mongolia, Heilongjiang, Sichuan, Shaanxi, and Gansu PLADs experienced particularly high levels of indirect economic burden. The impact of patients' labor loss and reduced productivity on indirect losses is substantial.

This study has two limitations. First, there is a lack of accepted studies providing disease weights specifically for KBD. Hence, we utilized the disability weights for other musculoskeletal disorders from the GBD 2019 as a suitable reference in our study (10). Second, the economic burden analysis in this study did not take into account the direct economic burden and intangible economic burdens associated with KBD. As

a result, the estimated economic burden of KBD may be underestimated.

In conclusion, while efforts have been made to control the current KBD epidemic, the disease and economic burden it poses are still substantial. Our study revealed that KBD was particularly severe in the western PLADs of China, with Sichuan Province having the highest YLD rate. The greatest proportion of YLDs occurred in patients with degree II of severity and individuals aged 60 and above. Shaanxi Province experienced the most severe indirect economic burden, with losses exceeding 30 million CNY. Gender did not significantly influence disease burden, but age was a crucial factor. These findings will aid the government in developing targeted prevention and control measures, as well as providing appropriate healthcare and financial assistance to areas affected by KBD. This will ultimately enhance the quality of life and economic well-being of patients.

Conflicts of interest: No conflicts of interest.

[#] Corresponding authors: Jun Yu, 6yujun@126.com; Junrui Pei, peijunrui@ems.hrbmu.edu.cn.

[1] NHC Key Laboratory of Etiology and Epidemiology (Harbin Medical University); Key Laboratory of Etiology and Epidemiology, Education Bureau of Heilongjiang Province; Institute of Kashin-Beck Disease Control, Center for Endemic Disease Control, Chinese Center for Disease Control and Prevention; Harbin Medical University, Harbin City, Heilongjiang Province, China; [2] NHC Key Laboratory of Etiology and Epidemiology (Harbin Medical University); Heilongjiang Provincial Key Laboratory of Trace Elements and Human Health, Key Laboratory of Etiology and Epidemiology, Education Bureau of Heilongjiang Province; Institute of Endemic Fluorosis Control, Center for Endemic Disease Control, Chinese Center for Disease Control and Prevention; Harbin Medical University, Harbin City, Heilongjiang Province, China.
[&] Joint first authors.

REFERENCES

1. Environmental and Endemic Disease Research Group, Institute of Geography, Chinese Academy of Sciences. Study on the relationship between the low selenium belt and the etiology of Keshan disease and macrosomia in China. Bull Chin Acad Sci 1988;3(1):54 – 60. http://dx.doi.org/10.16418/j.issn.1000-3045.1988.01.011. (In Chinese).
2. Guo X, Ma WJ, Zhang F, Ren FL, Qu CJ, Lammi MJ. Recent advances in the research of an endemic osteochondropathy in China: Kashin-Beck disease. Osteoarthritis Cartilage 2014;22(11):1774 – 83. http://dx.doi.org/10.1016/j.joca.2014.07.023.
3. National Monitoring Group for Kashin Beck Disease. The monitoring report of KBD prevalence rate of all country in 2000 year. Chin J Endemiol 2000;19(6):433 – 5. http://dx.doi.org/10.3760/cma.j.issn.1000-4955.2000.06.012. (In Chinese).
4. Qi F, Cui SL, Zhang B, Li HN, Yu J. A study on atypical Kashin-Beck disease: an endemic ankle arthritis.J Orthop Surg Res. 2023;23;18(1):379. http://dx.doi.org/10.1186/s13018-023-03860-z.
5. Maredza M, Bertram MY, Tollman SM. Disease burden of stroke in rural South Africa: an estimate of incidence, mortality and disability adjusted life years. BMC Neurol 2015;15:54. http://dx.doi.org/10.1186/s12883-015-0311-7.
6. Jia TW, Utzinger J, Deng Y, Yang K, Li YY, Zhu JH, et al. Quantifying quality of life and disability of patients with advanced schistosomiasis japonica. PLoS Negl Trop Dis 2011;5(2):e966. http://dx.doi.org/10.1371/journal.pntd.0000966.
7. Murray CJ, Kreuser J, Whang W. Cost-effectiveness analysis and policy choices: investing in health systems. Bull World Health Organ 1994;72(4):663-74. https://pubmed.ncbi.nlm.nih.gov/7923545/.
8. Cui SL, Deng Q, Pei JR, Jiao Z, Liu N, Cao YH, et al. Summary report of a national survey of Kashin-Beck disease prevalence in 2019. Chin J Endemiol 2021;40(7):545 – 50. http://dx.doi.org/10.3760/cma.j.cn231583-20201020-00270. (In Chinese).
9. Wang J, Wang XY, Li HR, Yang LS, Li YC, Kong C. Spatial distribution and determinants of health loss from Kashin-Beck disease in Bin County, Shaanxi Province, China. BMC Public Health 2021;21(1):387. http://dx.doi.org/10.1186/s12889-021-10407-6.
10. GBD 2019 Diseases and Injuries Collaborators. Global burden of 369 diseases and injuries in 204 countries and territories, 1990-2019: a systematic analysis for the Global Burden of Disease Study 2019. Lancet 2020;396(10258):1204 – 22. http://dx.doi.org/10.1016/S0140-6736(20)30925-9.